

The Structure of Hydrogenase-2 from *Escherichia coli*: Implications for H₂-driven Proton Pumping

Stephen E. Beaton¹, Rhiannon M. Evans¹, Alexander J. Finney², Ciaran M. Lamont²,

Fraser A. Armstrong^{1*}, Frank Sargent^{2*} and Stephen B. Carr^{3,4*}

¹Department of Chemistry, Inorganic Chemistry Laboratory, University of Oxford, Oxford OX1 3QR. ²Division of Molecular Microbiology, School of Life Sciences, University of Dundee, Dundee DD1 5EH, UK. ³Research Complex at Harwell, Rutherford Appleton Laboratory, Harwell Oxford, Didcot OX11 0FA, UK, ⁴Department of Biochemistry, University of Oxford, Oxford OX1 3QU, UK.

*Correspondence: fraser.armstrong@chem.ox.ac.uk; f.sargent@dundee.ac.uk; stephen.carr@rc-harwell.ac.uk

Abstract

Under anaerobic conditions *Escherichia coli* is able to metabolize molecular hydrogen via the action of several [NiFe]-hydrogenase enzymes. Hydrogenase-2, which is typically present in cells at low levels during anaerobic respiration, is a periplasmic-facing membrane-bound complex that functions as a proton pump to convert energy from H₂ oxidation into a proton gradient; consequently, its structure is of great interest. Empirically, the complex consists of a tightly-bound core catalytic module, comprising large (HybC) and small (HybO) subunits, which is attached to an Fe-S protein (HybA) and an integral membrane protein, HybB. To date, efforts to gain a more detailed picture have been thwarted by low native expression levels of hydrogenase-2 and the labile interaction between HybOC and HybA/HybB subunits. In this paper we describe a new over-expression system that has facilitated determination of high-resolution crystal structures of HybOC and, hence, a prediction of the quaternary structure of the HybOCAB complex.

Keywords: hydrogenase, metalloenzyme, *Escherichia coli*, iron-sulphur protein, protein structure

Abbreviations: Hyd-1, *E. coli* Hydrogenase-1 Hyd-2, *E. coli* Hydrogenase-2; IscR, iron-sulphur cluster regulator, MBH, membrane bound hydrogenase; Tat, Twin-arginine transporter; TM,

transmembrane; SEC-MALLS, size-exclusion chromatography with multi angle laser light scattering; PFE, protein film electrochemistry; EPR, electron paramagnetic resonance

Introduction

Hydrogen metabolism is an important feature of microbial physiology. In bacteria, molecular hydrogen (H_2) can be used as an electron donor during respiration and, conversely, proton reduction to H_2 is commonly employed to dispose of excess reducing equivalents during fermentation. Depending on the prevailing environmental conditions, the model organism *Escherichia coli* produces three [NiFe]-hydrogenase isoenzymes.[1] The unusual active site of [NiFe]-hydrogenases, the structure of which is remarkably conserved, has attracted a great deal of attention: it consists of a Ni atom which is coordinated by four cysteines, two of which are bridging to an Fe atom that is further coordinated by two CN^- and one CO ligand.[2,3] The bridging position between the Ni and Fe atoms can be occupied by a further ligand – a hydroxide in oxidized inactive states ('Ni-A' or 'Ni-B', as defined by characteristic EPR spectra, noting that Ni-A is modified further due to aerobic oxidation of active site cysteine to sulfenic acid)[4] or a hydride in active states ('Ni-C', 'Ni-R').[2] Minimally, [NiFe]-hydrogenases are comprised of a core catalytic heterodimer having a large subunit containing the active site and a small electron-transferring subunit that contains at least one Fe-S cluster.[2]

In *E. coli*, Hydrogenase-1 (Hyd-1) is produced under anaerobic conditions in the late stationary phase of cell growth and is a member of the Group 1d hydrogenases that are characterized as oxygen-tolerant hydrogen oxidizers or are linked directly to O_2 respiration.[1,5,6] Hydrogenase-3 (Hyd-3) is part of the formate hydrogenlyase complex that is produced under fermentative conditions and required for disproportionation of formate to CO_2 and H_2 :[1,7] it is classified as a Group 4 hydrogenase dedicated to H_2 evolution.[6] Finally, Hydrogenase-2 (Hyd-2) is a member of the Group 1c [NiFe]-hydrogenases that are involved in anaerobic respiration, are O_2 -sensitive, and are bidirectional in that they can oxidize or evolve hydrogen with high efficiency.[5,6,8–10] Importantly, Hyd-2 has been proposed to function as a H_2 -driven proton pump, and in this paper we describe investigations to elucidate its structure.

Hydrogenase-2 is encoded by the *hybOABCDEFG* operon[11,12] (Figure 1A) which is expressed under anaerobic respiratory conditions, and allows H_2 to be used as an electron

donor for fumarate reduction.[9,11,13] Expression of the *hyb* operon is repressed by nitrate[14] and by the action of the iron-sulfur cluster regulator 'IscR' under aerobic conditions.[15,16] The structural genes are *hybOABC*, where *hybC* encodes the large subunit (often referred to as α) and *hybO* encodes the small subunit (often referred to as β). The HybOC heterodimer is located at the periplasmic side of the inner membrane, where it is anchored by a single C-terminal transmembrane (TM) domain on the small subunit HybO (Figure S1).[17,18] The HybOC module also associates with HybA, a protein containing four [4Fe-4S] clusters that is anchored at the periplasmic side of the membrane by a C-terminal TM domain, and HybB, an integral membrane protein comprised of 10 TM helices (Figure S1).[1] The HybOC heterodimer is capable of both hydrogen oxidation and proton reduction, and the assumed role of HybAB is to couple this activity to the redox status of the quinone pool.[9]

In this paper, we report crystal structures of HybOC to high resolution, made possible by the design and optimization of a novel overexpression system for its increased production in *E. coli*. We compare the electrochemical and enzymatic profiles of the overproduced enzyme with native Hyd-2, which show it is essentially identical. Finally, consideration of the possible interactions of HybOC with homology models of HybA and HybB leads to a proposal for the complete structure of the membrane-bound complex.

Experimental

Molecular Biology.

E. coli K-12 strains used in this work (Table S1) are based on MC4100.[19] IC011 (as MC4100, \DeltahyaB , \DeltahycE , \DeltahybOA) and HJ001 (as IC011 \DeltaiscR) have been previously described.[20] The HJ001-hyp strain was prepared by first cloning a synthetic *hypA1-X* operon, based on the sequences of *R. eutropha* [NiFe]-hydrogenase maturases,[20] into pFAT122[21] as an EcoRI/Sall fragment. This strain was then combined with a Sall/KpnI fragment from pFAT123[21] resulting in a pBluescript (Amp^R) vector carrying a $\Delta tatD::hypA1-X$ allele. The entire $\Delta tatD::hypA1-X$ allele was then transferred as an XbaI/KpnI fragment to pMAK705 and transferred to the chromosome of HJ001 as described.[22] The resultant HJ001-hyp strain carries the entire synthetic *hypA1-X* operon in place of *tatD*, which has no known role in hydrogenase

activity.[21] The *hybO* gene was amplified from a colony suspension of strain FTH013 using primers AmplifyHybO_F and AmplifyHybO_R (see Table S1). The resulting PCR product was composed of *hybO* without the N-terminal Tat sequence (i.e. starting at codon 38, Glu) and without the C-terminal TM domain such that HybO is truncated at codon 330 (Gly) and immediately followed by the C-terminal his-tag. The amplification primers also encoded an overlapping region complementary to plasmid pQE-80L. The pQE-80L plasmid was amplified using primers OpenpQE80_F and OpenpQE80_R which contained complementary regions, overlapping with the amplified *hybO* PCR product. The two fragments were assembled using standard protocols via Gibson assembly and the resultant plasmid called pO^C.

Enzyme Production and Purification.

Native Hyd-2 (Hyd-2-N) for all electrochemical (PFE) and viologen-based assays was produced and purified from strain FTH013 using a previously published procedure.[23] Strain FTH013 was cultured anaerobically at 37 °C in Luria broth supplemented with glycerol (0.5% w/v) and sodium fumarate (0.4 % w/v). Cells were harvested in late exponential phase (9 hours following inoculation, 1% inoculum used), resuspended in Tris 100 mM, pH 7.5, EDTA 1mM, NaCl 50 mM, with added DNase (0.003% w/v) and lysozyme (0.012% w/v), and frozen at -80 °C. Purification of Hyd-2-N relied on the chromosomally-encoded C-terminal his-tag on *hybO*: cells were thawed at room temperature and lysed by two passes through a cell disruptor system (Constant Systems) at 20 kPSI. Unbroken cells were pelleted by centrifugation at 3750 rpm and passed through a cell disruptor at 25 kPSI. Cell membranes were pelleted from the lysed cells by ultracentrifugation at 45000 rpm, 4 °C for 60 mins and resuspended in Tris (100 mM, pH 7.5), NaCl (350 mM), before being mechanically homogenized by hand. The homogenized membranes were solubilized in Triton X-100 (to 3% v/v) stirring for 40 mins at 4 °C, and debris pelleted at 45000 rpm for 60 mins at 4 °C. Imidazole (40 mM) and DTT (1 mM) were added to the resulting supernatant solution before it was applied to a Ni-affinity column (5 mL column volume, His-trap HP, GE Healthcare), pre-equilibrated with Tris (20 mM, pH 7.2), NaCl (350 mM), imidazole (60 mM), Triton X-100 (0.02% v/v), DTT (1 mM). Following a 20 column-volume wash to remove unbound protein, Hyd-2-N was eluted from the Ni-affinity column by imidazole gradient (60 mM to 750 mM) over 16 column volumes. Fractions were assessed for content and

purity by the absorbencies at 280 nm and 420 nm and by SDS-PAGE electrophoresis, pooled and concentrated using centrifugal concentrators with a 50,000 molecular weight cut-off (Vivaspin).

For electrochemical analyses, the concentrated Hyd-2-N was buffer exchanged (PD-10 desalting columns, GE Healthcare) into Tris (50 mM, pH7.2), NaCl (350 mM), Triton X-100 (0.02% v/v), glycerol (10% v/v), DTT (1 mM) and snap-frozen in N₂(l).

Recombinant, overproduced Hyd-2 (Hyd-2-NOP) was produced from *E. coli* HJ001-hyp transformed with pO^C plasmid. Cells were grown anaerobically in Luria Broth with 0.5% (v/v) glycerol and 0.4% (w/v) sodium fumarate, with added ampicillin (to 100 µg/mL). Transcription from the plasmid was induced by isopropyl β-D-1-thiogalactopyranoside (IPTG, final concentration 1 mM) at an OD₆₀₀ of 0.25. Cells were harvested 9 hours after induction in the late exponential phase, resuspended and frozen as outlined above. Purification of Hyd-2-NOP followed the previously published procedure for ΔTM hydrogenases:[23] frozen cell pellets were thawed at room temperature and protease inhibitor tablets were added (cOmplete, mini EDTA-free protease inhibitor cocktail, Roche, 1 tablet per 30 L culture) and allowed to stir into solution for 20 minutes at 4 °C. Cells were lysed by two passes through a cell disruptor system (Constant Systems) at 20 kPSI. Debris was pelleted by ultracentrifugation at 45000 rpm for 30 mins at 4 °C. Imidazole (50 mM) and DTT (1 mM) were added to the resulting supernatant solution before being applied to a Ni-affinity column (5 mL column volume, His-trap FF Crude, GE Healthcare) pre-equilibrated with Tris (50 mM, pH 7.2), NaCl (350 mM), imidazole (50 mM), DTT (1 mM). Unbound proteins were washed from the column over 20 column volumes. A 16 column volume imidazole gradient (50 to 500 mM) was used to elute Hyd-2-NOP. Fractions were assessed for content and purity by the absorbencies at 280 nm and 420 nm and by SDS-PAGE electrophoresis, then pooled and concentrated using centrifugal concentrators with a 50,000 molecular weight cut-off (Vivaspin).

For electrochemical analyses, the concentrated Hyd-2-NOP was buffer exchanged (PD-10 desalting columns, GE Healthcare) into Tris (50 mM, pH7.2), NaCl (350 mM), glycerol (10% v/v), DTT (1 mM) and snap-frozen in liquid nitrogen. For structural analyses, the concentrated

Hyd-2-NOP was buffer exchanged (PD-10 desalting columns, GE Healthcare) into Tris (20 mM, pH7.2), NaCl (150 mM), DDM (0.02% w/v), DTT (1 mM) before further purification by size exclusion chromatography (Superdex 200 Increase 10/300, GE Healthcare). Fractions were assessed for content and purity by the absorbencies at 280 nm and 420 nm and by SDS-PAGE electrophoresis, pooled and concentrated using centrifugal concentrators with a 50,000 molecular weight cut-off (Vivaspin) to a concentration of 5 mgmL⁻¹, and determined using the method of Bradford.[24]

Rocket immunoelectrophoresis.

E. coli strains IC011, HJ001 and HJ001-hyp were separately transformed with pO^N or pO^C. The cells were then cultured anaerobically in sealed 500 mL Duran bottles containing LB medium supplemented with 0.5% (v/v) glycerol, 0.4% (w/v) sodium fumarate, 50 µg/ml ampicillin and 1 mM IPTG from the outset. Following growth at 37 °C for 16 hours cells were harvested by centrifugation, washed in 50 mM Tris.HCl (pH 8.0) and suspended at 1 g cell paste (wet weight) to 10 ml 50 mM Tris.HCl (pH 8.0). Cell suspensions were then lysed by sonication, and cell debris and membranes removed by ultracentrifugation. To prepare the gel, a 1% (w/v) agarose suspension was prepared in 20 mM sodium barbitone (pH 8.3) buffer. To 5 ml of this suspension was added 5 µL of a Hyd-2 rabbit serum raised against Hyd-2-N as purified previously[5] from strain FTH013 (see Table S1). The mixture was then poured over a 5 cm × 5 cm glass plate and allowed to set before 2 mm diameter wells were inserted using a leather hole punch. Next, 2 µl of protein sample was added to each well and the agarose plates subjected to electrophoresis for 16 hours at 2 mA *per* plate using 20 mM sodium barbitone (pH 8.3) as buffer (4 °C). Following electrophoresis, the plates were removed and incubated in 50 mM Tris.HCl (pH 7.5) containing 0.5 mM benzyl viologen and 1 mM tetrazolium red under a 100% H₂ atmosphere, typically for 12 hours at 37 °C or until red formazan precipitate became visible.

Protein Film Electrochemistry.

Protein film electrochemistry is a technique in which small amounts of hydrogenase are adsorbed onto a suitable working electrode for measurement of enzyme activity under

controlled potential. The all-glass electrochemical cell was located inside an anaerobic glovebox (MBraun; $[O_2] < 0.5$ ppm.). A three-electrode configuration was used, in which a saturated calomel reference electrode (SCE) was located in a side arm connected to the main compartment of the cell by a luggin capillary. The main compartment, equipped with gas inlet and outlet ports and typically accommodating 2 mL of buffer-electrolyte solution, housed the pyrolytic graphite 'edge' (PGE) working electrode (which could be rotated at high speed) and a Pt counter electrode. For each experiment, the PGE (geometric surface area 0.03 cm^2) was sanded (Hookit P400 sand paper) and hydrogenase solution ($0.5\text{--}2\text{ }\mu\text{L}$ at $1\text{--}5\text{ mg/ml}$) was applied by repeated 'add/withdraw' pipetting for 30 seconds as previously described. The electrode was then rinsed with ultrapure H_2O (Millipore, $18\text{ M}\Omega\text{ cm}$) to remove unabsorbed protein, and attached to the electrode rotator motor.[25] Potential values were converted to the standard hydrogen electrode (SHE) scale ($E_{SCE} = E_{SHE} + 0.241\text{ V}$ at 25°C) to allow easy comparison with published biochemical data.[26]

Solution Assays.

Solution assays determining the rate of hydrogen oxidation were carried out following an established procedure.[25] A micro-Eppendorf tube of the enzyme was placed under a 100% H_2 environment for 12-24 hours to ensure full reductive activation of the enzyme. To measure H_2 oxidation activity, the reduction of 2 mM benzyl viologen ($E=-358$, $\epsilon = 8.4\text{ mM}^{-1}\text{ cm}^{-1}$ at 604 nm)[27] was monitored at 604 nm under anaerobic conditions in a sealed cuvette containing 1 mL of K_iPO_4 buffer at 6.0 pH saturated with H_2 . An appropriate quantity of the enzyme ($1\text{--}10\text{ }\mu\text{g}$) was injected to initiate the reaction. The solution was stirred for the duration of the reaction. The enzyme was then placed under 100% Ar for at least 12 hours. To measure H_2 production, the oxidation of 0.40 mM fully reduced methyl viologen ($E=-446$, $\epsilon=13.9\text{ mM}^{-1}\text{ cm}^{-1}$ at 604 nm)[27] was monitored at 604 nm under anaerobic conditions in a sealed cuvette containing 1 mL of K_iPO_4 buffer at pH 6.0 saturated with Ar.

SEC-MALLS

A sample of Hyd-2-NOP at a concentration of 5 mgmL^{-1} was injected into a superdex S200 increase column connected to an Akta pure chromatography system. Data were collected using

a flow rate of 0.5 mL min^{-1} . Light scattering measurements were collected using a Dawn Helios-II (Wyatt Technologies, USA) and refractive index measured using an Optilab T-rex refractometer (Wyatt Technologies, USA). Scattering data were analyzed using the conjugate analysis module in the Astra package. Conjugate analysis uses the light scattering signal in combination with the UV and refractive index signals to differentiate between scattering from protein and detergent, enabling the molecular weight of the protein embedded in the detergent micelle to be accurately determined. The extinction coefficient of the protein was calculated from the amino acid sequence, while that of DDM was taken to be zero. The dn/dc values used in the analysis were 0.185 mL g^{-1} for protein and 0.143 mL g^{-1} for DDM.

Protein crystallisation

Following Ni-affinity and size exclusion chromatography, purified Hyd-2-NOP was concentrated to 5 mg mL^{-1} using centrifugal concentrators with a 50,000 molecular weight cut-off (Vivaspin). Protein concentration was assessed by Bradford assay.⁴¹ Crystals of Hyd-2-NOP were obtained using the sitting drop vapour diffusion technique, whereby 100 nL of protein solution was mixed with an equal volume of crystallisation solution using a Mosquito robot (TTP labtech, UK) followed by incubation at 293 K in an aerobic atmosphere. Crystals of H₂-reduced Hyd-2 were obtained in a similar manner, but the Hyd-2 solution was exposed to an atmosphere of 100% hydrogen to activate the enzyme prior to crystallisation in an anaerobic glove box containing a 100% nitrogen atmosphere. Long rod-shaped crystals appeared within 24 hours from a mixture of Bis-tris (100 mM, pH 5.5), MgCl₂ (200 mM) and PEG 3350 (25% w/v). Prior to x-ray data collection, crystals were manually transferred to a cryoprotecting solution of Bis-tris (100 mM, pH 5.5), MgCl₂ (200 mM), PEG 3350 (27% w/v) and glycerol (15% v/v) for 60 s before flash-cooling by immersion in liquid nitrogen.

X-ray data collection and structure determination

Diffraction data for the as-isolated enzyme were collected at beamline P14, PETRA III (Hamburg) at a wavelength of 0.976 \AA using a Pilatus 6M hybrid pixel array detector, whereas data for the reduced enzyme were collected at beamline I03 (Diamond Light Source, UK) at a wavelength of 0.9794 \AA using a Pilatus 6M detector. All data sets were collected at 100 K using

a helical line scan to minimise photo-reduction during exposure to x-rays. All data reduction was performed using DIALS[28] and Aimless.[29] Initial phase estimates for the as-isolated enzyme were generated using Phaser[30] with pdb file 5A4M as a search model. Initial electron density maps were fragmented and difficult to interpret, manual addition of [4Fe4S] clusters in the proximal position and resetting the occupancy of the other metal centres using COOT[31] followed by 50 cycles of all atom refinement in REFMAC5[32] greatly improved the electron density allowing automated model building using BUCCANEER.[33] Subsequent rounds of modelling and refinement were performed manually using COOT and REFMAC5 using TLS restraints and isotropic B-factors. Phase estimates for the reduced structures were calculated by rigid-body positional refinement of the as-isolated Hyd-2 model into the unit cell of the reduced structures using REFMAC5 followed by iterative rounds of manual rebuilding (COOT) and restrained refinement (REFMAC5). Structure superpositions were performed using LSQKAB[34] and analysis of protein interfaces was carried out using PISA.[35] The occupancy of the SD oxygen atom at Cys546 was estimated by deleting the carbonyl oxygen atom of nearby residue Arg428 (an atom present at 100% occupancy) and the SD oxygen atom of Cys546. Electron density maps were recalculated for the structure with the missing atoms followed by comparison of the relative heights of the Fo-Fc map peaks for the missing O atoms.

Results

Overproduction of Hyd-2 catalytic core

HybO and HybA are synthesized as precursor proteins with N-terminal twin-arginine (Tat) signal peptides for periplasmic targeting, and both also carry C-terminal TM domains for attachment to the membrane.[18] These structural and biosynthetic features limit the amount of Hyd-2 found in the cell at native levels ($0.015 \text{ mg of Hyd-2 (g of cells)}^{-1}$).[5] Previous strategies to purify Hyd-2 have involved protease treatment of membranes, which cleaved the HybO TM and liberated an active fragment of Hyd-2 (HybOC).[17] Similarly, detergent solubilisation of membranes with inclusion of a chromosomally-encoded hexa-histidine affinity tag (His-tag) on the C-terminus of HybO (strain FTH013 in this study denoted Hyd-2-N and used in all electrochemical comparisons, see Figure 1A, and Table S1), allowed isolation of HybOC, with a

small amount of co-purifying HybA.[5] In order to increase the yield of active Hyd-2 for biochemical and structural experiments, we designed an innovative overexpression system.

In principle, overproduction of HybOC should be possible if all cofactor biosynthesis, cofactor insertion, and enzyme maturation processes are kept in perfect balance. Moreover, previous work suggested that cellular levels of the small subunit (HybO) may be a limiting factor in Hyd-2 assembly, since excess large subunit (HybC) was often found in the cytoplasm in anaerobically-grown cells.[36] This observation suggested that overexpression of the *hybO* gene encoding the small subunit alone could be a useful strategy. To test this hypothesis, an *E. coli* mutant strain was chosen (IC011, Table S1) which lacked the genes for the Hyd-1 and Hyd-3 large subunits and also carried in-frame, non-polar deletions in *hybO* and *hybA*. [20] Although still encoding the Hyd-2 large subunit HybC, this strain has no hydrogenase activity. Thus, when a soluble protein extract was examined by Rocket immunoelectrophoresis,[13,37] no dye-linked Hyd-2 activity was detected (Figure 2A). Next, two plasmids were prepared that encoded truncated, His-tagged versions of *E. coli* HybO. Both plasmids encode *hybO* with a truncation of the C-terminal TM domain at codon 330 and deletion of the N-terminal Tat signal. The plasmid pO^N has an N-terminal His-tag, whereas pO^C has a C-terminal His-tag (Table S1).

The *E. coli* IC011 strain was transformed with either empty vector, pO^N, or pO^C and grown anaerobically in the presence of 1 mM IPTG before a soluble protein extract was prepared. Under identical conditions, a control strain ('FTD674', Table S1) producing a soluble version of Hyd-2 at native levels[18] was also cultured, and the relative amounts of active Hyd-2 were then assessed by Rocket immunoelectrophoresis[13,37] and Western immunoblotting (Figure 2A,C). Under these conditions, direct replacement of the HybO Tat signal peptide with an N-terminal His-tag (pO^N) led to poor protein production and no Hyd-2 activity. However, the plasmid encoding signal-less HybO carrying a C-terminal His-tag (pO^C) produced stable small subunit that was able to interact with the large subunit (HybC) and generate an active Hyd-2 enzyme. Moreover, the amount of enzyme produced by the plasmid-based system exceeded native levels.

To boost, further, the yield of recombinant Hyd-2 to levels that would facilitate structural characterization by X-ray crystallography, an innovative combination of genetic engineering strategies was adopted. Not only is the *hyb* operon repressed by *IscR*, [15] but removal of the *iscR* gene has proven beneficial for overproduction of Fe-S cluster containing proteins. [38] A version of the IC011 strain carrying a Δ *iscR* allele (HJ001) [20] was transformed with pO^N or pO^C . Once more, the inclusion of an N-terminal His-tag appeared detrimental to protein stability and enzyme assembly, whereas the strain producing HybO with a C-terminal His-tag generated active Hyd-2 in excess of that observed for the native enzyme (Figure 2A).

To maximize [NiFe]-cofactor biosynthesis capability for HybC in the host strain, *hyaB* and *hycE*, which encode the large Ni- and Fe-containing subunits of Hyd-1 and Hyd-3, respectively, were deleted. It has previously been shown that a synthetic version of the *Ralstonia eutropha* *hypA1B1F1C1D1E1X* operon, encoding cofactor maturases, is active in *E. coli*. [20] A version of the *hypA1-X* operon, including the constitutive *E. coli* *tat* promoter, [20] was integrated into the chromosome of strain HJ001 at the non-essential *tatD* locus to give the new strain 'HJ001-hyp' (see Figure 1B and Table S1). The pO^N and pO^C plasmids were then used to transform HJ001-hyp and the cells were cultured under anaerobic overexpression conditions. Analysis of the soluble cell fractions revealed that active Hyd-2 was produced at high levels in this host strain, so long as the plasmid encoding C-terminally His-tagged HybO was used (Figure 2B, C). Based on these results, a protocol was developed (see Methods) that resulted, reproducibly, in an order-of-magnitude increase in production of Hyd-2, i.e. approximately 0.15 mg of Hyd-2 (g of cells)⁻¹.

Purification and Catalytic Activity of Recombinant Hyd-2

Based on the high yield of protein purified from the cytoplasm of HJ001-Hyp with pO^C (produced from strain HJ001-hyp. pO^C) and termed 'Hyd-2-NOP' (NOP = native, overproduced), this combination of strain and plasmid was used to overproduce protein for structural characterization (Figure S2). A full enzymatic characterization was performed for Hyd-2-NOP, to ensure that the protein was fully formed and functionally comparable to Hyd-2-N, which is

isolated from the periplasmic membrane having undergone full post-translational maturation and has previously been extensively characterised.⁵

Protein film electrochemistry (PFE) produces, in a single experiment, a characteristic profile of the catalytic oxidation and reduction activities of an enzyme that is adsorbed on an electrode. In cyclic voltammetry, the electrode potential is cycled between two limits and the resulting catalytic activity is directly measured as current.[39–42] The previously published electrochemical profile of Hyd-2-N showed it to be a reversible hydrogenase for which proton reduction is inhibited by the product H₂. [5,10] The electrochemical profile of recombinant, overproduced Hyd-2-NOP adsorbed on a pyrolytic graphite edge (PGE) electrode is also consistent with these characteristics, in that the enzyme requires only a minimal overpotential to catalyze either H₂ oxidation or H⁺ reduction. The catalytic cyclic voltammogram of Hyd-2-NOP cuts sharply through the zero-current axis, and the H⁺ reduction current decreases with increasing H₂ partial pressure (see Figure S3, Figure S4, Figure S5, and Figure S6 for full electrochemical measurements and comparison).

The electrochemical profiles of Hyd-2-N and Hyd-2-NOP are similar despite the fact that the Hyd-2-N HybOC catalytic core is co-purified with variable amounts of HybA,[5] a protein containing a relay chain of four Fe-S clusters (Figure S1): conversely, *hybA* is deleted from the chromosome of strain HJ001-hyp, used to produce Hyd-2-NOP. Clearly, the presence of HybA has a negligible effect on the shape of the electrochemical profile.

The EPR spectra for samples of Hyd-2-NOP prepared under different conditions (Figure S7) are identical to those published for Hyd-2-N.[5,43] Turnover frequencies obtained by conventional assays are also within error for the two enzymes. Additionally, Hyd-2-N and Hyd-2-NOP share key metrics of enzymatic activity, and steady-state kinetic parameters are in good agreement with those previously published for Hyd-2-N (Table 1).

Structure of recombinant overproduced Hyd-2

Overall fold

The crystal structure of recombinant Hyd-2-NOP produced using the new strategy was solved to a maximum resolution of 1.5 Å (reduced) or 2.2 Å (as-isolated) (Table 2). Reduced structures were generated in either of two ways: by exposing Hyd-2-NOP to a 100% H₂ atmosphere for 12 hours prior to crystallization, or by addition of 5 mM DTT to the cryoprotecting solution and soaking as-isolated crystals for 1-2 minutes prior to flash cooling. All structures reveal, as previously predicted (native PAGE and analytical ultracentrifugation, AUC, measurements),^[17] that the catalytic core of Hyd-2 is a dimer of heterodimers (Figure 3, [HybOC]₂ – for clarity in this specific case, we use this notation instead of (αβ)₂). This arrangement is similar to that observed previously for O₂-tolerant hydrogenases^[44–46] (also reviewed in reference^[47]) and recently for the Actinobacterial-like-[NiFe]-hydrogenase from *R. eutropha*.^[48] Analysis of the HybOC subunits using the DALI server (http://ekhidna.biocenter.helsinki.fi/dali_server/)^[49] shows that they display a classic oxidoreductase fold similar to [NiFe]-hydrogenases from a wide variety of organisms and nearly identical to the fold of *E. coli* Hyd-1 (Figure S8).³² The dimer of heterodimers is stabilized by 17 salt bridges and a further 16 hydrogen bonds in an extensive interface that spans both copies of the small and large subunits and buries 2678 Å² of the solvent-accessible surface. Analysis of Hyd-2-NOP by SEC-MALLS (Size Exclusion Chromatography with Multi-Angle Laser Light Scattering) in the presence of detergent confirmed the stability of the [HybOC]₂ dimer with only minimal amounts of enzyme present in the HybOC monomeric form (Figure 4). The two copies of the HybOC dimer in the asymmetric unit show clear electron density for residues 10-276 (of 293+6 His giving 299) of HybO and for residues 2-552 (of 552) of HybC. Since residues 277-299 of HybO were still present in the crystals (Figure S9), the lack of visible density suggests they are flexible and disordered in the crystal lattice.

Large subunit

Each HybOC heterodimer contains a NiFe catalytic centre within the large (HybC) subunit. The Ni and Fe atoms in the active site are coordinated by four cysteine thiolate ligands (Cys61, Cys64, Cys546 and Cys549) and three of the remaining coordination positions of the Fe are occupied by small inorganic ligands (2 CN[−] and CO). The active site is structurally identical to that of Hyd-1^[44] with the similarity extending into the 'canopy' residues (Asp103, Arg479 and

Asp554) above the active site, which comprise part of the second coordination sphere (Figure S10).

Residual electron density occupying the bridging position between Ni and Fe was assigned to a hydroxide ligand in the as-isolated enzyme, since the proteins were purified aerobically. The bridging hydroxide was visible in both as-isolated and chemically reduced protein, an observation that can be explained in terms of the difficulty in activating enzyme that is in the unready state, and the need for H₂ to be present in addition to a supply of electrons.[2] Both as-isolated and chemically reduced crystals showed evidence for oxygenation of Cys546 (Figure S10).[4]

In the H₂-reduced structure there is no evidence for oxygenation of any of the coordinating thiolate groups and the distance between the Ni and Fe atoms has decreased from 2.85 to 2.65 Å. Repositioning of the Ni atom causes the coordinating thiolates (Cys61 and Cys546) to rotate approximately 10° towards the metal atom, resulting in a contraction of the active site cavity that allows the carboxylate group of residue Glu14 to move 0.35 Å closer to the NiFe centre. Residue Glu14 is the equivalent residue to Glu28 in Hyd-1 that has been shown to be essential for proton-coupled electron transfer.[50] A small peak in the Fo-Fc difference electron density is observed in the bridging position in one active site, and superposition of the Ni-R form of the NiFe center from *D. vulgaris* Miyazaki F (pdb:4U9H)[51] places the hydrogen atom located in that study within the difference density. The reduced *D. vulgaris* enzyme also has a similar separation of the Ni and Fe atoms at the catalytic centre. A similar sized peak is also observed between the Ni and Fe atoms in the second active site, but its centroid is located much closer to the Ni (1.6 Å) than the Fe atom (2.45 Å) and superposition of the Ni-R catalytic centre of pdb:4U9H does not place the hydrogen atom in the density (Figure S11). Similar to most Group 1 [NiFe]-hydrogenases, during maturation, the final 15 amino acids encoded at the C-terminal of HybC are proteolytically processed[52] leaving a C-terminal His (552) to bind to a structural magnesium ion.[2,53] The structure of HybC confirms the presence of a magnesium ion coordinated by His552, Glu42 and the main chain carbonyl of Ala498.

Small subunit

As for all other Group 1 [NiFe]-hydrogenases, the small subunit (HybO) contains three iron-sulphur clusters that are separated from each other by a maximum distance of 10.7 Å and thus well suited to mediate rapid long-range electron transfer to and from the active site in HybC (Figure S12).[54] Interestingly, the dimer of heterodimers structure places the two distal clusters within 12.3 Å of each other, implying that interdomain electron transfer could occur between each HybOC module.[54] The distal [4Fe-4S] cluster is located close to the surface of the small subunit and is coordinated by three cysteine residues (Cys195, Cys220 and Cys225) and one histidine (His192). The medial [3Fe-4S] cluster forms the central part of the electron-transfer chain and is coordinated by Cys235, Cys255 and Cys258. The electron transfer chain in all group 1 [NiFe]-hydrogenases has a [3Fe-4S] cluster in the medial position, with the exception of the relative small group of NiFeSe sub-class of group 1a, where it is replaced by a [4Fe-4S] cluster.

The proximal [4Fe-4S] cluster, that closest to the catalytic NiFe centre, displays standard cubane geometry in both the chemically reduced and H₂ reduced structures and is completely coordinated by cysteine ligands (Cys22, Cys25, Cys120 and Cys154). Additional features were visible in the 2Fo-Fc map close to the proximal cluster for the as-isolated enzyme following prolonged exposure to air during protein purification (Figure 5). Anomalous difference density maps showed that these features were caused by movement of an Fe atom and the result was interpreted in terms of oxidative disruption of the cluster, similar to that observed for the [NiFe]-hydrogenase of *A. vinosum* and *D. desulfuricans*. [55,56] Interestingly, as the Fe atom moves away from the rest of the cluster and loses its coordination contact with Cys25, a nearby aspartate residue (Asp81) rotates to coordinate the Fe in its new position. From the relative intensities of the peaks in the anomalous difference maps for the migrated Fe, approximately 50% of the protein molecules in the crystal are modified in this way.

Discussion

The low expression levels and subsequent poor yield of *E. coli* Hyd-2 has hampered detailed biochemical investigations of this enzyme. Overproduction of multi-subunit, multi-cofactor

metalloenzymes is challenging and often requires carefully coordinated co-expression of large numbers of accessory genes.[57] In the case of *E. coli* Hyd-2, we reasoned that one limiting factor was the availability of the Fe-S-cluster-containing small subunit (HybO) of the central catalytic core, since Western immunoblots showed the large subunit (HybC) is present in excess in the cytoplasm.[36] To this end, we developed an overexpression system that allowed us to obtain greatly-enhanced amounts of active Hyd-2 suitable for a full biochemical and structural characterization. In terms of host strain development, in-frame and unmarked deletions in *hybOA* would not be expected to affect transcription and translation of the downstream *hybBCDEFG* genes. Strains without the *hybOA* allele have no Hyd-2 activity, clearly showing, in agreement with the work of Pinske *et al.*,[58] that the large subunit HybC is unable to exhibit benzyl viologen-linked H₂-oxidation activity without its small subunit partner. Introduction of *hybO* alone on a plasmid was sufficient not only to restore Hyd-2 activity but also to boost the amount of Hyd-2 in the cell an order of magnitude above native levels. Importantly, the version of HybO studied here was completely devoid of the N-terminal Tat signal peptide and C-terminal TM domain, thus demonstrating that, for this type of Tat substrate, the signal peptide probably has no additional role in enzyme biosynthesis beyond protein targeting.

Further host strain engineering, by de-repression of Fe-S cluster biosynthesis (and *hyb* operon expression), and by supplying additional copies of NiFe cofactor biosynthesis proteins, led to a highly active protein product. The new enzyme form contains a full complement of metal cofactors with enzymatic characteristics in excellent agreement with those for the native enzyme.

The active site region is very similar to that of the H₂-oxidizing homologue Hyd-1, supporting proposals that characteristic properties of specific [NiFe]-hydrogenases, such as O₂ tolerance[59–61] and bias with regard to H₂ oxidation vs H₂ evolution,[62–65] are determined much more by the nature of the iron-sulfur clusters that supply or remove electrons. Comparisons between the as-isolated and H₂-reduced structures show that the oxygenated sulfur and bridging hydroxide ligand are no longer present in the latter. The H₂-reduced structure also shows contraction of the Ni–Fe distance and small movements of the polypeptide backbone surrounding the NiFe center: notably, Glu14 moves towards the NiFe

center, potentially improving the rate of proton transfer in and out of the active site. The position of side chains of other ionisable groups that could facilitate subsequent proton-transfer steps to and from the active site remain unchanged, implying that the proton-transfer pathway is close to optimal. The reduced structures are likely to be a mix of reduced intermediates from the catalytic cycle similar to the mixture observed in the EPR samples (Figure S7), yet, the active site of one HybOC heterodimer appears to be predominantly in the Ni-R form, since the active site residues are structurally identical and the residual electron density peak is coincident with the bridging hydride in the Ni-R state of *D. vulgaris* Myazaki F.[51] The second active site may represent another state in the catalytic cycle, since the residual electron density peak is no longer in the bridging position, but much closer to the Ni atom, however, spectroscopic or EPR validation would be required to confirm this. The alternative proximal cluster configuration has been observed previously,[55,56] and sequence alignment of group 1 hydrogenases reveals an aspartate, glutamate or asparagine residue is conservatively substituted in position 81 (Figure S13). The repositioning of the acidic side chain could be advantageous since coordination by aspartate prevents the loss of Fe from the proximal cluster upon oxidative damage, and addition of reducing equivalents allows reconstitution of the [4Fe-4S] cluster.

Evidence for a dimer-of-heterodimers configuration in vivo

The dimer of heterodimers configuration of the large and small subunits ([HybOC]₂), with distal cluster close enough to allow efficient inter-subunit electron tunneling, seen in Hyd-2 has previously been exclusively linked with O₂-tolerance having only been observed in O₂-tolerant hydrogenases.[44–46] A dimeric structure has also recently been proposed for the standard O₂-sensitive hydrogenase from *A. vinosum*,[47,55] however, the distance between distal clusters is too large to allow inter-subunit electron tunneling. Also the free energy of dissociation (ΔG^{diss}) of the dimer of heterodimers (calculated using PISA[50]) is 16 kcal/mol for the *A. vinosum* enzyme suggesting this quaternary structure is less stable than in [HybOC]₂, where (ΔG^{diss}) is 23.0 kcal/mol, similar to that calculated for the O₂-tolerant-membrane-bound hydrogenase from *H. marinarus*.³¹ For comparison (ΔG^{diss}) of the obligate heterodimer HybOC

in Hyd-2 was found to be approximately 52.0 kcal/mol (52 kcal/mol for *A. vinosum*) These calculations represent a lower limit based on the interactions seen in the crystal structure. The equilibrium constant for dimerization of the HybOC heterodimers is therefore approximately 10^{17} — a value which suggests Hyd-2 exists naturally in a dimer-of-heterodimers configuration. Previous analytical ultracentrifugation experiments also suggested the [HybOC]₂ configuration was stable in aqueous solution at a range of protein concentrations.[17] Moreover, the SEC-MALLS results of Hyd-2-NOP in the presence of detergent (Figure 4), a condition that should favor the monomeric HybOC heterodimer form, provide additional compelling support for the inherent stability of the [HybOC]₂ dimer in solution, leading to the conclusion that it represents the *in vivo* structure.

Hyd-2 as a proton pump: a model for the quaternary structure of membrane-bound Hyd-2 complex

Most membrane-bound hydrogenases are thought to couple H₂ oxidation to quinone reduction with the concomitant transmembrane translocation of protons, conserving energy as a proton gradient. Membrane-bound hydrogenases such as *E. coli* Hyd-1 and the *R. eutropha* MBH achieve this by associating the core hydrogenase subunits with an integral membrane cytochrome *b*, which contains one haem close to the hydrogenase distal [Fe-S] cluster and a second haem at the cytoplasmic side of the membrane near the quinone binding site. These hydrogenases operate as scalar proton pumps where redox reactions separated by the ion-impermeable inner membrane result in a net translocation of protons. Hyd-2 belongs to a different and little-studied class of hydrogenases that are true conformational proton pumps. The proposed proton-pumping activity, involves the membrane-embedded HybB protein in coupling the energy released from H₂-dependent menaquinone reduction to generation of a transmembrane proton gradient. By analogy with structurally-defined homologous proteins,[66] HybB does not contain haem or any other metal cofactors and the menaquinone binding site is located at the periplasmic side of the membrane. Cycles of menaquinone binding, reduction, and menaquinol release are thought to drive conformational changes in the membrane protein that powers proton translocation. Compelling evidence for this with *E. coli* Hyd-2 is derived from studies of the reverse reaction.[9] If the quinone pool becomes over-

reduced, for example, by the presence of plentiful electron donors and an absence of electron acceptors, Hyd-2 can transduce energy stored in the proton gradient to catalyze the menaquinol-dependent reduction of protons to H_2 . This reversed electron transport is completely inhibited by the addition of chemical uncouplers that collapse the transmembrane proton electrochemical gradient.[9]

The Hyd-2 holoenzyme is predicted to comprise the HybOC dimer together with HybA and HybB. An intact HybOCAB enzyme has never been isolated, suggesting protein-protein associations beyond the catalytic core are more labile. The primary stabilizing force of Hyd-2 is the interaction between HybO and HybC in the heterodimer followed by the dimeric interaction of $[HybOC]_2$. Although the crystal structure presented represents only the catalytic core of Hyd-2, it provides important insight into the quaternary structure of the HybOCAB complex within the bacterial membrane. The stability of the $[HybOC]_2$ dimer and the location of hydrophobic patches on the surface of HybOC (that could mediate protein-protein interactions, Figure S14) being central in guiding the construction of a model for the quaternary complex.

To construct a plausible model for the HybOCAB complex structures for HybA and HybB were produced by homology modelling using the Phyre 2 server.[67]. These were particularly informative, since the protein templates used are themselves components of other membrane-anchored multi-protein respiratory enzymes and therefore not only suggest the individual structures of HybA and HybB, but also their probable location within the larger HybOCAB complex. For example, the FdnH ferredoxin subunit of formate dehydrogenase (pdb: 1kqf),[68] used to model HybA, sits between a dehydrogenase catalytic subunit and a quinone-reactive integral membrane protein, elevating the catalytic subunit away from the surface of the membrane. Assuming the HybA subunits adopt a similar position in HybOCAB gives important clues to the architecture of HybOCAB. Biochemical experiments point to the C-terminal TM of HybA interacting with the C-terminal TM of HybO.[5] Moreover, the distal [Fe-S] cluster of HybO must be located within 15 Å of the proximal cluster of HybA in order for efficient electron transfer to occur. The proposed location of HybA is consistent with these observations, implying the catalytic HybOC dimer must be positioned further away from the membrane face than would be the case in either *E. coli* Hyd-1 or *R. eutropha* MBH. Comparison of the crystal

structure with the protein sequence reveals that the HybO C-terminal helix, which anchors HybO to the cytoplasmic membrane and interacts with the HybA TM, is separated from the C-terminus of the catalytic domain by a linker comprised of 17 amino acids (not observed in the electron density maps). This linker is sufficiently long to allow HybA to be positioned between the catalytic HybOC complex and the membrane surface and still allow interaction between the HybO and HybA TM helices.[5] This model, also places the distal cluster of HybO within 13.5 Å of one of the Fe-S clusters of HybA, close enough to allow electron transfer between the two proteins,[54] and in the equivalent position to the cluster that accepts electrons from the MoCo active site in FndH. Further supporting the proposal that HybA acts as an electron-transfer relay between HybOC and the integral membrane protein HybB that is expected to contact the quinone pool. Positioning of a ferredoxin subunit between a catalytic subunit and an integral membrane component is observed in other membrane-associated redox complexes, including polysulfide reductase[66] and nitrate reductase.[69] Typically, the catalytic and ferredoxin subunits are present in a 1:1 ratio [66, 68, 69], suggesting there are two copies of HybA in the HybOCAB complex.

HybB is an integral membrane protein which is proposed to contain the menaquinone binding site and also to act as a conformational proton pump.[9,66] Homology modelling[67] using PsrC, the integral membrane component of polysulfide reductase (pdb: 2vpz),[66] as a template reveals a structure with eight of the predicted TM helices arranged in two four-helix-bundle-like folds. The polysulfide reductase complex consists of two PsrABC trimers with PsrC providing almost all the interactions that stabilize the dimer interface, suggesting that HybB would also tend to dimerize in the membrane.

The stability of the [HybOC]₂ dimer of heterodimers, the implied propensity of HybB to dimerize, and the observation that in other redox complexes each catalytic subunit has its own partner ferredoxin, suggests strongly that the physiological complex of Hyd-2 comprises two copies of each protein [HybOCAB]₂, (Figure 6). The organisation of proteins in the model of Hyd-2 can be divided into 3 distinct modules; an outer catalytic module, a central electron relay module and an integral membrane module linking H₂ oxidation/production to the quinone pool.

Such an arrangement is seen in a variety of other membrane-anchored, multi-subunit redox protein complexes including nitrate reductase and even Complex I.[69–71]

Interrogation of the [HybOCAB]₂ model (Figure 6) will allow the mechanism of proton pumping to be determined. For example, it is likely that electron transfer from HybA to the quinone binding site on HybB is by a highly conserved mechanism. Studies of both polysulfide reductase[66] and DMSO reductase[72] identified a conserved proline residue important in regulating electron transfer to quinone. The equivalent conserved residue in HybA is Pro-125, is an obvious start point for further investigation.

The role of Hyd-2 in infection and colonization

Membrane-bound hydrogenases of the HybOCAB type are crucial enzymes for understanding H₂ metabolism in bacterial pathogens. Interest in Hyd-2 therefore extends beyond its capability for efficient H₂ production, to understanding its unique mechanism of linking H₂ metabolism to the pathogenicity of microorganisms. As such, the determination of high resolution crystal structures of Hyd-2 is a major step forward and will be essential to the characterization of hydrogenase inhibitors designed to combat infections.[73]

Hyd-2 is especially important in the food- and water-borne pathogen *Salmonella enterica* where it has dual roles in both infection and colonization.[74,75] In *S. enterica*, Hyd-2 activity also contributes to virulence in a mouse model:[74,76] Moreover, Hyd-2 was found to be critical for anaerobic growth of *S. enterica* in environments designed to simulate the gut lumen where the proton motive force generated by Hyd-2 was used for rapid uptake of amino acids.[77] In this same vein, Hyd-2 is important in the specific colonization of some animal hosts. A large-scale genomic study discovered that *S. enterica* carrying inactivating mutations in the *hybOABCDEFG* operon was unable to colonize the chicken gut, but was completely unaffected in the ability to colonize cattle or pigs.[75]

The structure of HybOC determined here is already giving new impetus to the study of the molecular basis of Hyd-2 in virulence. An *S. enterica* strain commonly used in laboratory-based studies is the attenuated non-pathogenic LT2a strain. Sequencing of this strain identified a Gly-153-Asp substitution in HybO close to the Cys-154 ligand to the proximal [4Fe-4S] cluster.[78]

Analysis of the structure shows the backbone torsion angles of the polypeptide chain in this region are only accessible to glycine and mutation to any other amino acid would disrupt the proximal and medial Fe-S clusters or their immediate environment, resulting in the non-pathogenic phenotype.

In conclusion, the overexpression system developed here establishes that HybO availability is an important limiting factor for native Hyd-2 synthesis and that HybO Δ TAT Δ TM can be expressed from a plasmid with negligible effects on enzymatic activity. This new approach will facilitate mutagenesis and other molecular biology techniques for subunits expressed from the plasmid. Moreover, as shown, successful overproduction of a single [NiFe]-hydrogenase subunit provides a new strategy for increasing yields of hydrogenase or other proteins processed by the Tat system, with obvious advantages for their biophysical and biochemical analysis. Lastly, the structure of the catalytic core of Hyd-2 provides valuable insight both as the structure affects the catalytic activity of HybOC and as the basis for a prediction of the quaternary structure with its own physiological implications.

Acknowledgements

We would like to thank Diamond Light Source for beamtime (proposal mx12346) and the staff of beamline I03 for assistance during data collection, PETRA III for beamtime and the staff of beamline P14 for help during data collection. We also thank Dr Edward Lowe for collecting x-ray diffraction data for the as-isolated enzyme and Dr Gemma Harris for collection and analysis of the SEC-MALLS data. We are grateful to Dr. Will Myers for his assistance in the collection of EPR spectra as well as the CAESR Facility at the University of Oxford. Mrs Elena Nomerotskaia is acknowledged for invaluable technical assistance throughout this work.

Declaration of interests

The authors state there are no conflicts of interest.

Funding information

This research was funded in Oxford by the Biotechnology and Biological Sciences Research Council (BBSRC) Grant BB/N006321/1, and in Dundee by BBSRC EASTBIO Doctoral Training Partnership awards 1510231 and 1280664. FAA is a Royal Society Wolfson Research Merit Award holder. SEB is grateful to the Dakota Foundation for the award of a Holaday Scholarship.

Author Contributions

SEB generated plasmid and strain constructs, purified protein and carried out biochemical and electrochemical analysis under the supervision of RME. SBC crystallized Hyd-2, collected x-ray diffraction data and solved the structure. FS and AJF performed cloning, rocket immunoelectrophoresis assays and Western immunoblotting, while FS and CML performed strain construction. FAA and RME conceived the study and the manuscript was written by SEB, RME, SBC, FS and FAA.

References

- 1 Sargent, F. (2016) The Model [NiFe]-Hydrogenases of *Escherichia coli*. In *Advances in Microbial Physiology*, pp 433–507.
- 2 Lubitz, W., Ogata, H., Rudiger, O. and Reijerse, E. (2014) Hydrogenases. *Chem. Rev.* **114**, 4081–4148.
- 3 Fontecilla-Camps, J. C., Volbeda, A., Cavazza, C. and Nicolet, Y. (2007) Structure/function relationships of [NiFe]- and [FeFe]-hydrogenases. *Chem. Rev.* **107**, 4273–4303.
- 4 Volbeda, A., Martin, L., Barbier, E., Gutierrez-Sanz, O., De Lacey, A. L., Liebgott, P. P., Dementin, S., Rousset, M. and Fontecilla-Camps, J. C. (2015) Crystallographic studies of [NiFe]-hydrogenase mutants: Towards consensus structures for the elusive unready oxidized states. *J. Biol. Inorg. Chem.* **20**, 11–22.
- 5 Lukey, M. J., Parkin, A., Roessler, M. M., Murphy, B. J., Harmer, J., Palmer, T., Sargent, F. and Armstrong, F. A. (2010) How *Escherichia coli* is equipped to oxidize hydrogen under different redox conditions. *J. Biol. Chem.* **285**, 3928–3938.
- 6 Greening, C., Biswas, A., Carere, C. R., Jackson, C. J., Taylor, M. C., Stott, M. B., Cook, G. M. and Morales, S. E. (2016) Genomic and metagenomic surveys of hydrogenase distribution indicate H₂ is a widely utilised energy source for microbial growth and survival. *ISME J., Nature Publishing Group* **10**, 761–777.
- 7 McDowall, J. S., Murphy, B. J., Haumann, M., Palmer, T., Armstrong, F. A. and Sargent, F. (2014) Bacterial formate hydrogenlyase complex. *Proc. Natl. Acad. Sci.* **111**, E3948–E3956.
- 8 Trchounian, K., Soboh, B., Sawers, R. G. and Trchounian, A. (2013) Contribution of Hydrogenase 2 to Stationary Phase H₂ Production by *Escherichia coli* During Fermentation of Glycerol. *Cell Biochem. Biophys.* **66**, 103–108.
- 9 Pinske, C., Jaroschinsky, M., Linek, S., Kelly, C. L., Sargent, F. and Sawers, R. G. (2015) Physiology and bioenergetics of [NiFe]-hydrogenase 2-catalyzed H₂-consuming and H₂-producing reactions in *Escherichia coli*. *J. Bacteriol.* **197**, 296–306.
- 10 Armstrong, F. a and Hirst, J. (2011) Reversibility and efficiency in electrocatalytic energy conversion and lessons from enzymes. *Proc. Natl. Acad. Sci. U. S. A.* **108**, 14049–54.
- 11 Menon, N. K., Chatelus, C. Y., Dervartanian, M., Wendt, J. C., Shanmugam, K. T., Peck, H. D. and Przybyla, A. E. (1994) Cloning, sequencing, and mutational analysis of the *hyb* operon encoding *Escherichia coli* hydrogenase 2. *J. Bacteriol., American Society for Microbiology* **176**, 4416–23.
- 12 Sargent, F., Ballantine, S. P., Rugman, P. A., Palmer, T. and Boxer, D. H. (1998) Reassignment of the gene encoding the *Escherichia coli* hydrogenase 2 small subunit - identification of a soluble precursor of the small subunit in a *hypB* mutant. *Eur. J. Biochem.* **255**, 746–754.

- 13 Ballantine, S. P. and Boxer, D. H. (1985) Nickel-containing hydrogenase isozymes from anaerobically grown *Escherichia coli* K-12. *J Bacteriol* **163**, 454–459.
- 14 Richard, D. J., Sawers, G., Sargent, F., McWalter, L. and Boxer, D. H. (1999) Transcriptional regulation in response to oxygen and nitrate of the operons encoding the [NiFe] hydrogenases 1 and 2 of *Escherichia coli*. *Microbiology* **145**, 2903–2912.
- 15 Giel, J. L., Rodionov, D., Liu, M., Blattner, F. R. and Kiley, P. J. (2006) IscR-dependent gene expression links iron-sulphur cluster assembly to the control of O₂-regulated genes in *Escherichia coli*. *Mol. Microbiol.*, Blackwell Publishing Ltd **60**, 1058–1075.
- 16 Nesbit, A. D., Giel, J. L., Rose, J. C. and Kiley, P. J. (2009) Sequence-Specific Binding to a Subset of IscR-Regulated Promoters Does Not Require IscR Fe–S Cluster Ligation. *J. Mol. Biol.* **387**, 28–41.
- 17 Ballantine, S. P. and Boxer, D. H. (1986) Isolation and characterisation of a soluble active fragment of hydrogenase isoenzyme 2 from the membranes of anaerobically grown *Escherichia coli*. *Eur. J. Biochem.* **156**, 277–284.
- 18 Hatzixanthis, K., Palmer, T. and Sargent, F. (2003) A subset of bacterial inner membrane proteins integrated by the twin-arginine translocase. *Mol. Microbiol.* **49**, 1377–1390.
- 19 Casadaban, M. J. and Cohen, S. N. (1979) Lactose genes fused to exogenous promoters in one step using a Mu-lac bacteriophage: In vivo probe for transcriptional control sequences **76**, 4530–4533.
- 20 Lamont, C. M. and Sargent, F. (2016) Design and characterisation of synthetic operons for biohydrogen technology. *Arch. Microbiol.*, Springer Berlin Heidelberg **199**, 495–503.
- 21 Wexler, M., Sargent, F., Jack, R. L., Stanley, N. R., Bogsch, E. G., Robinson, C., Berks, B. C. and Palmer, T. (2000) TatD is a cytoplasmic protein with DNase activity. No requirement for TatD family proteins in sec-independent protein export. *J. Biol. Chem.*, American Society for Biochemistry and Molecular Biology **275**, 16717–22.
- 22 Hamilton, C. M., Aldea, M., Washburn, B. K., Babitzke, P. and Kushner, S. R. (1989) New method for generating deletions and gene replacements in *Escherichia coli*. *J. Bacteriol.*, American Society for Microbiology **171**, 4617–22.
- 23 Evans, R. M., Brooke, E. J., Wehlin, S. A. M., Nomerotskaia, E., Sargent, F., Carr, S. B., Phillips, S. E. V and Armstrong, F. A. (2015) Mechanism of hydrogen activation by [NiFe] hydrogenases. *Nat. Chem. Biol.*, Nature Publishing Group **12**, 46–50.
- 24 Bradford, M. M. (1976) A rapid and sensitive method for the quantitation of microgram quantities of protein utilizing the principle of protein-dye binding. *Anal. Biochem.*, Academic Press **72**, 248–254.
- 25 Brooke, E. J., Evans, R. M., Islam, S. T. A., Roberts, G. M., Wehlin, S. A. M., Carr, S. B., Phillips, S. E. V. and Armstrong, F. A. (2017) Importance of the Active Site “Canopy” Residues in an O₂-Tolerant [NiFe]-Hydrogenase. *Biochemistry* **56**, 132–142.

- 26 Bard, A. J., Faulkner, L. R., York, N., @bullet, C., Brisbane, W. and Toronto, S. E. (1944) Electrochemical Methods: Fundamentals and Applications. Electrochem. Methods Fundam. Appl.
- 27 Cammack, R., Fernandez, V. M. and Hatchikian, E. C. (1994) Nickel Iron Hydrogenase. In Methods Enzymology, pp 43–68.
- 28 Waterman, D. G., Winter, G., Gildea, R. J., Parkhurst, J. M., Brewster, A. S., Sauter, N. K. and Evans, G. (2016) Diffraction-geometry refinement in the *DIALS* framework. Acta Crystallogr. Sect. D Struct. Biol., International Union of Crystallography **72**, 558–575.
- 29 Evans, P. R. and Murshudov, G. N. (2013) How good are my data and what is the resolution? Acta Crystallogr. Sect. D Biol. Crystallogr., International Union of Crystallography **69**, 1204–1214.
- 30 McCoy, A. J., Grosse-Kunstleve, R. W., Adams, P. D., Winn, M. D., Storoni, L. C. and Read, R. J. (2007) Phaser crystallographic software. J. Appl. Crystallogr., International Union of Crystallography **40**, 658–674.
- 31 Emsley, P., Lohkamp, B., Scott, W. G. and Cowtan, K. (2010) Features and development of Coot. Acta Crystallogr. Sect. D Biol. Crystallogr., International Union of Crystallography **66**, 486–501.
- 32 Murshudov, G. N., Skubák, P., Lebedev, A. A., Pannu, N. S., Steiner, R. A., Nicholls, R. A., Winn, M. D., Long, F. and Vagin, A. A. (2011) REFMAC5 for the refinement of macromolecular crystal structures. Acta Crystallogr. Sect. D Biol. Crystallogr. **67**, 355–367.
- 33 Cowtan, K. (2006) The Buccaneer software for automated model building. 1. Tracing protein chains. Acta Crystallogr. Sect. D Biol. Crystallogr., International Union of Crystallography **62**, 1002–1011.
- 34 Kabasch, W. (Max-P.-I. fur M. F. (1976) A solution for the best rotation to relate two sets of vectors. Acta Crystallogr. **32**, 922–923.
- 35 Krissinel, E. and Henrick, K. (2007) Inference of Macromolecular Assemblies from Crystalline State. J. Mol. Biol. **372**, 774–797.
- 36 Dubini, A., Pye, R. L., Jack, R. L., Palmer, T. and Sargent, F. (2002) How bacteria get energy from hydrogen: A genetic analysis of periplasmic hydrogen oxidation in Escherichia coli. Int. J. Hydrogen Energy **27**, 1413–1420.
- 37 Sawers, R. G., Ballantine, S. P. and Boxer, D. H. (1985) Differential expression of hydrogenase isoenzymes in Escherichia coli K-12 : evidence for a third isoenzyme . Differential Expression of Hydrogenase Isoenzymes in Escherichia coli K-12 : Evidence for a Third Isoenzyme **164**, 1324–1331.
- 38 Kuchenreuther, J. M., Grady-Smith, C. S., Bingham, A. S., George, S. J., Cramer, S. P. and Swartz, J. R. (2010) High-Yield Expression of Heterologous [FeFe] Hydrogenases in

- Escherichia coli*. PLoS One (Tyagi, A. K., ed.), Public Library of Science **5**, e15491.
- 39 Armstrong, F. A., Evans, R. M., Hexter, S. V., Murphy, B. J., Roessler, M. M. and Wulff, P. (2016) Guiding Principles of Hydrogenase Catalysis Instigated and Clarified by Protein Film Electrochemistry. *Acc. Chem. Res.* **acs.accounts.6b00027**.
- 40 Vincent, K. A., Parkin, A. and Armstrong, F. A. (2007) Investigating and exploiting the electrocatalytic properties of hydrogenases. *Chem. Rev.* **107**, 4366–4413.
- 41 Armstrong, F. A., Belsey, N. A., Cracknell, J. A., Goldet, G., Parkin, A., Reisner, E., Vincent, K. A. and Wait, A. F. (2009) Dynamic electrochemical investigations of hydrogen oxidation and production by enzymes and implications for future technology. *Chem. Soc. Rev.*, Royal Society of Chemistry **38**, 36–51.
- 42 Léger, C. and Bertrand, P. (2008) Direct Electrochemistry of Redox Enzymes as a Tool for Mechanistic Studies. *Chem. Rev.*, American Chemical Society **108**, 2379–2438.
- 43 Roessler, M. M. (2012) EPR Investigations of Iron-Sulfur Cluster Relays in Enzymes. *Dep. Inorg. Chem.*
- 44 Volbeda, A., Amara, P., Darnault, C., Mouesca, J.-M., Parkin, A., Roessler, M. M., Armstrong, F. A. and Fontecilla-Camps, J. C. (2012) X-ray crystallographic and computational studies of the O₂-tolerant [NiFe]-hydrogenase 1 from *Escherichia coli*. *Proc. Natl. Acad. Sci. U. S. A.* **109**, 5305–10.
- 45 Fritsch, J., Scheerer, P., Frielingsdorf, S., Kroschinsky, S., Friedrich, B., Lenz, O. and Spahn, C. M. T. (2011) The crystal structure of an oxygen-tolerant hydrogenase uncovers a novel iron-sulphur centre. *Nature* **479**, 249–252.
- 46 Shomura, Y., Yoon, K.-S., Nishihara, H. and Higuchi, Y. (2011) Structural basis for a [4Fe-3S] cluster in the oxygen-tolerant membrane-bound [NiFe]-hydrogenase. *Nature, Nature Research* **479**, 253–256.
- 47 Wulff, P., Thomas, C., Sargent, F. and Armstrong, F. A. (2016) How the oxygen tolerance of a [NiFe]-hydrogenase depends on quaternary structure. *JBIC J. Biol. Inorg. Chem.* **121**–134.
- 48 Schäfer, C., Bommer, M., Hennig, S. E., Jeoung, J. H., Dobbek, H. and Lenz, O. (2016) Structure of an Actinobacterial-Type [NiFe]-Hydrogenase Reveals Insight into O₂-Tolerant H₂ Oxidation. *Structure* **24**, 285–292.
- 49 Holm, L. and Ivi Rosenströ, P. Dali server: conservation mapping in 3D.
- 50 Dementin, S., Burlat, B., De Lacey, A. L., Pardo, A., Adryanczyk-Perrier, G., Guigliarelli, B., Fernandez, V. M. and Rousset, M. (2004) A Glutamate is the Essential Proton Transfer Gate during the Catalytic Cycle of the [NiFe] Hydrogenase. *J. Biol. Chem.* **279**, 10508–10513.
- 51 Ogata, H., Nishikawa, K. and Lubitz, W. (2015) Hydrogens detected by subatomic resolution protein crystallography in a [NiFe] hydrogenase. *Nature* **520**, 571–4.

- 52 Dubini, A. and Sargent, F. (2003) Assembly of Tat-dependent [NiFe] hydrogenases: Identification of precursor-binding accessory proteins. *FEBS Lett.* **549**, 141–146.
- 53 Higuchi, Y., Yagi, T. and Yasuoka, N. (1997) Unusual ligand structure in Ni – Fe active center and an additional Mg site in hydrogenase revealed by high resolution X-ray structure analysis. *Structure* **5**, 1671–1680.
- 54 Page, C. C., Moser, C. C., Chen, X. and Dutton, P. L. (1999) Natural engineering principles of electron tunnelling in biological oxidation-reduction. *Nature* **402**, 47–52.
- 55 Ogata, H., Kellers, P. and Lubitz, W. (2010) The crystal structure of the [NiFe] hydrogenase from the photosynthetic bacterium *allochromatium vinosum*: Characterization of the oxidized enzyme (Ni-A state). *J. Mol. Biol., Elsevier Ltd* **402**, 428–444.
- 56 Matias, P. M., Soares, C. M., Saraiva, L. M., Coelho, R., Morais, J., Le Gall, J. and Carrondo, M. A. (2001) [NiFe] hydrogenase from *Desulfovibrio desulfuricans* ATCC 27774: Gene sequencing, three-dimensional structure determination and refinement at 1.8 Å and modelling studies of its interaction with the tetrahaem cytochrome c3. *J. Biol. Inorg. Chem.* **6**, 63–81.
- 57 Schiffels, J., Pinkenburg, O., Schelden, M., Aboulmaga, E.-H. A. A., Baumann, M. E. M. and Selmer, T. (2013) An Innovative Cloning Platform Enables Large-Scale Production and Maturation of an Oxygen-Tolerant [NiFe]-Hydrogenase from *Cupriavidus necator* in *Escherichia coli*. *PLoS One* (Battista, J. R., ed.), Public Library of Science **8**, e68812.
- 58 Pinske, C., Krüger, S., Soboh, B., Ihling, C., Kuhns, M., Braussemann, M., Jaroschinsky, M., Sauer, C., Sargent, F., Sinz, A., et al. (2011) Efficient electron transfer from hydrogen to benzyl viologen by the [NiFe]-hydrogenases of *Escherichia coli* is dependent on the coexpression of the iron–sulfur cluster-containing small subunit. *Arch. Microbiol., Springer-Verlag* **193**, 893–903.
- 59 Lukey, M. J., Roessler, M. M., Parkin, A., Evans, R. M., Davies, R. A., Lenz, O., Friedrich, B., Sargent, F. and Armstrong, F. A. (2011) Oxygen-tolerant [NiFe]-hydrogenases: The individual and collective importance of supernumerary cysteines at the proximal Fe-S cluster. *J. Am. Chem. Soc.* **133**, 16881–16892.
- 60 Evans, R. M., Parkin, A., Roessler, M. M., Murphy, B. J., Adamson, H., Lukey, M. J., Sargent, F., Volbeda, A., Fontecilla-Camps, J. C. and Armstrong, F. A. (2013) Principles of sustained enzymatic hydrogen oxidation in the presence of oxygen -the crucial influence of high potential Fe-S clusters in the electron relay of [NiFe]-hydrogenases. *J. Am. Chem. Soc.* **135**, 2694–2707.
- 61 Cracknell, J. a, Wait, A. F., Lenz, O., Friedrich, B. and Armstrong, F. a. (2009) A kinetic and thermodynamic understanding of O₂ tolerance in [NiFe]-hydrogenases. *Proc. Natl. Acad. Sci. U. S. A.* **106**, 20681–20686.
- 62 Hexter, S. V., Grey, F., Happe, T., Climent, V. and Armstrong, F. a. (2012) Electrocatalytic

- mechanism of reversible hydrogen cycling by enzymes and distinctions between the major classes of hydrogenases. *Proc. Natl. Acad. Sci.* **109**, 11516–11521.
- 63 Hexter, S. V, Esterle, T. F. and Armstrong, F. A. (2014) A unified model for surface electrocatalysis based on observations with enzymes. *Phys. Chem. Chem. Phys.* **16**, 11822–11833.
 - 64 Murphy, B. J., Sargent, F. and Armstrong, F. a. (2014) Transforming an oxygen-tolerant [NiFe] uptake hydrogenase into a proficient, reversible hydrogen producer. *Energy Environ. Sci.* **7**, 1426–1433.
 - 65 Adamson, H., Robinson, M., Wright, J. J., Flanagan, L. A., Walton, J., Elton, D., Gavaghan, D. J., Bond, A. M., Roessler, M. M. and Parkin, A. (2017) Retuning the Catalytic Bias and Overpotential of a [NiFe]-Hydrogenase via a Single Amino Acid Exchange at the Electron Entry/Exit Site. *J. Am. Chem. Soc., American Chemical Society* **139**, 10677–10686.
 - 66 Jormakka, M., Yokoyama, K., Yano, T., Tamakoshi, M., Akimoto, S., Shimamura, T., Curmi, P. and Iwata, S. (2008) Molecular mechanism of energy conservation in polysulfide respiration. *Nat. Struct. Mol. Biol., Nature Publishing Group* **15**, 730–737.
 - 67 Kelly, L. A., Mezulis, S., Yates, C., Wass, M. and Sternberg, M. (2015) The Phyre2 web portal for protein modelling, prediction, and analysis. *Nat. Protoc., Nature Publishing Group* **10**, 845–858.
 - 68 Jormakka, M., Törnroth, S., Byrne, B. and Iwata, S. (2002) Molecular Basis of Proton Motive Force Generation: Structure of Formate Dehydrogenase-N. *Science (80-.)*. **295**.
 - 69 Bertero, M. G., Rothery, R. A., Palak, M., Hou, C., Lim, D., Blasco, F., Weiner, J. H. and Strynadka, N. C. J. (2003) Insights into the respiratory electron transfer pathway from the structure of nitrate reductase A. *Nat. Struct. Biol., Nature Publishing Group* **10**, 681–687.
 - 70 Baradaran, R., Berrisford, J. M., Minhas, G. S. and Sazanov, L. A. (2013) Crystal structure of the entire respiratory complex I. *Nature, Nature Publishing Group* **494**, 443–448.
 - 71 Zhu, J., Vinothkumar, K. R. and Hirst, J. (2016) Structure of mammalian respiratory complex I. *Nature, Nature Publishing Group* **536**, 354–358.
 - 72 Victor W. T. Cheng, ‡, Richard A. Rothery, ‡, Michela G. Bertero, §, Natalie C. J. Strynadka, § and Joel H. Weiner*, ‡. (2005) Investigation of the Environment Surrounding Iron–Sulfur Cluster 4 of *Escherichia coli* Dimethylsulfoxide Reductase†, American Chemical Society .
 - 73 Nie, W., Tang, H., Fang, Z., Chen, J., Chen, H. and Xiu, Q. (2012) Hydrogenase: the next antibiotic target? *Clin. Sci. (Lond)., Portland Press Limited* **122**, 575–80.
 - 74 Maier, R. J., Olczak, A., Maier, S., Soni, S. and Gunn, J. (2004) Respiratory hydrogen use by *Salmonella enterica* serovar Typhimurium is essential for virulence. *Infect. Immun., American Society for Microbiology* **72**, 6294–9.
 - 75 Chaudhuri, R. R., Morgan, E., Peters, S. E., Pleasance, S. J., Hudson, D. L., Davies, H. M.,

- Wang, J., van Diemen, P. M., Buckley, A. M., Bowen, A. J., et al. (2013) Comprehensive Assignment of Roles for *Salmonella* Typhimurium Genes in Intestinal Colonization of Food-Producing Animals. *PLoS Genet.* **9**.
- 76 Zbell, A. L., Maier, S. E. and Maier, R. J. (2008) *Salmonella enterica* serovar Typhimurium NiFe uptake-type hydrogenases are differentially expressed in vivo. *Infect. Immun.*, American Society for Microbiology **76**, 4445–54.
- 77 Lamichhane-Khadka, R., Kwiatkowski, A. and Maier, R. J. (2010) The Hyb hydrogenase permits hydrogen-dependent respiratory growth of *Salmonella enterica* serovar Typhimurium. *MBio*, American Society for Microbiology **1**, e00284-10.
- 78 Pinske, C. and Sawers, R. G. (2016) Anaerobic Formate and Hydrogen Metabolism. *EcoSal Plus* **7**.
- 79 Karplus, P.A. & Deiderichs, K. Linking crystallographic Model and Data Quality Science, **336**, 1030-1033 (2012).

Figures and Tables

Table 1: Key enzymatic parameters for Hyd-2-N and Hyd-2-NOP, showing good agreement between the two enzymes.

Parameter	Hyd-2-N	Hyd-2-NOP
solution assay oxidation turnover frequency using benzyl viologen (s^{-1})^a	204 ± 26	218 ± 26
solution assay H_2 production turnover frequency using methyl viologen (s^{-1})^a	6 ± 2	5 ± 1
$K_M^{H_2}$ at -0.175 V (μM)^b	20 ± 5	24 ± 8
ΔH^\ddagger at -0.200 V ($kJ\ mol^{-1}$)^c	45 ± 2	43 ± 2
E_{switch} (mV)^d	-51 ± 10	-37 ± 27
$K_i^{H_2}$ at -0.670 V (μM)^c	219 ± 14	240 ± 11

^aAll measurements were carried out at pH 6.0 ^bMeasured at room temperature (20 °C). ^csee Figure S3, S4, S5, and S6 for details. ^dMeasured at 30°C.

Table 2. X-ray data collection and refinement statistics for Hyd-2-NOP.

Data collection			
Sample	As-Isolated/aerobic	Chemically Reduced	Hydrogen Reduced
PDB ID	6EHQ	6EHS	6EN9
Space group	$P2_12_12_1$	$P2_12_12_1$	$P2_12_12_1$
Unit cell dimensions (Å)	a=99.06, b=100.09, c=168.14	a=99.89, b=100.07, c=168.80	a=99.60, b=100.54, c=168.58
Resolution (Å)	85.4 – 2.2 (2.24-2.10)	65.2- 1.5 (1.53-1.50)	86.35-1.5 (1.53-1.50)
Total reflections	549,679 (27,487)	2,394,760 (111,154)	1,380,818 (74,652)
Unique reflections	84,222 (4,242)	269,411 (12,174)	255,707 (13,573)
Completeness (%)	98.7 (95.5)	100 (99.9)	99.2 (98.2)
Multiplicity	6.5 (6.5)	8.9 (8.4)	5.4 (5.5)
$\langle I/\sigma \rangle$	6.4 (1.7)	11.2 (1.4)	10.9 (1.6)
R _{merge} (%)	19.0 (98)	10.8 (145)	7.3 (85.8)
R _{pim} (%)	12.0 (62.9)	5.6 (79.5)	3.9 (43.9)
CC _{1/2}	0.978 (0.681)	0.998 (0.554)	0.998 (0.714)
Refinement			
R _{work} /R _{free} (%)	16.3/18.9	15.6/18.4	15.2/17.5
No. of atoms	13,242	13,570	13,903
Macromolecule	12,718	12,723	12,723
Solvent	524	847	1,180
Average B-factors			
Macromolecule	30.6	19.85	19.28
Solvent	29.2	24.26	25.7
RMSD bond lengths (Å)	0.0128	0.0167	0.017
RMSD angles (°)	1.53	1.72	1.78
Ramachandran plot (%) favoured / outliers	96.3 / 0	96.3/ 2	96.3/0
Clashscore	0.44	1.57	1.42

Values in parentheses refer to data in the highest resolution shell. Resolution limits for the refined model were determined using the paired refinement protocol⁷⁹

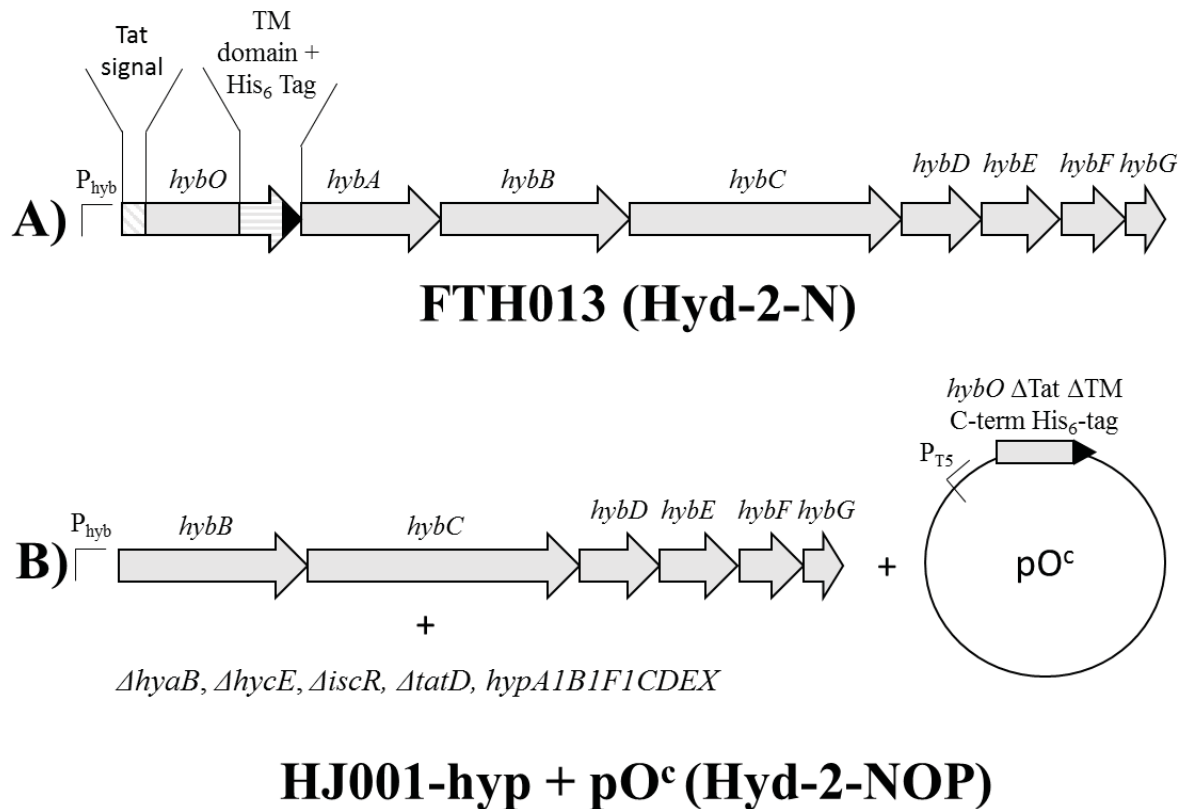


Figure 1: A) A representation of the engineered *hyb* operon of strain FTH013[5] used for Hyd-2-N production. B) A representation of the genotype of overexpression host strain HJ001-hyp that carries in-frame $\Delta hybOA$ and is transformed with plasmid pO^c : this was used to produce Hyd-2-NOP. See Table S1 for more information on plasmids and strains.

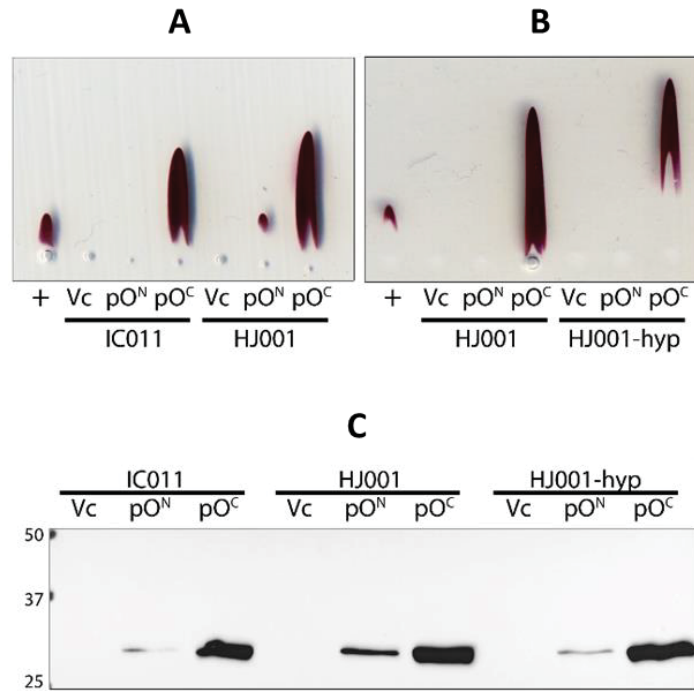


Figure 2: Overproduction of active Hyd-2 using a plasmid-encoded small subunit.

(A and B) Non-denaturing Rocket immunoelectrophoresis was performed using horizontal thin-layers of 1% (w/v) agarose containing 5 μ l of anti-Hyd-2 serum buffered with 20 mM barbitone-HCl at pH 8.3. Following electrophoresis, activity staining with 10 mM Tris-HCl pH 7.5 containing 0.5 mM benzyl viologen and 1 mM tetrazolium red was carried out under a 100% H₂ atmosphere. Soluble protein extracts of the FTD674 strain producing truncated Hyd-2 were applied as positive controls (+), and three different host strains IC011 (Δ hyaB, Δ hycE, Δ hybOA), HJ001 (Δ hyaB, Δ hycE, Δ hybOA, Δ iscR), and HJ001-hyp (Δ hyaB, Δ hycE, Δ hybOA, Δ iscR, Δ tatD::hypA1-X) were transformed with either pQE-80L vector (Vc) pQE-80L with hybO Δ Tat Δ TM N-terminal his-tag (pO^N), or pQE-80L with hybO Δ Tat Δ TM C-terminal his-tag (pO^C). **(C)** Identical soluble extracts used in (A, B) were also analyzed by Western immunoblotting (anti-his-tag antibody) following separation by SDS-PAGE and transfer to nitrocellulose.

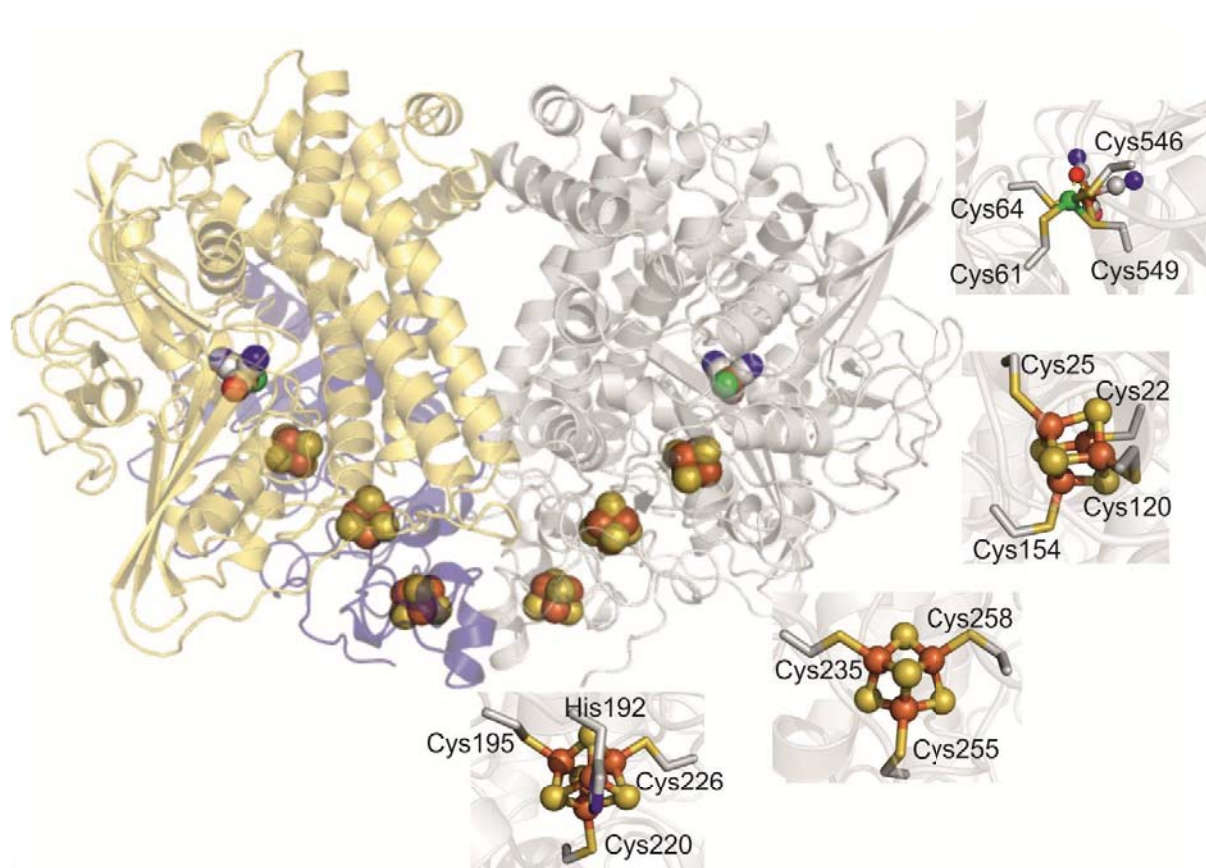


Figure 3: The structure of the catalytic core of Hyd-2-NOP containing two copies of the large and small subunits arranged as a dimer of heterodimers ($[\text{HybOC}]_2$). In one heterodimer the small subunit (HybO) is colored blue and the large subunit (HybC) gold, in the second, both subunits are shown in gray to accentuate the position of the metals centers, (displayed as spheres with iron-sulfur clusters colored bronze/yellow and the NiFe center bronze/green). Panels show the coordination of each metal center.

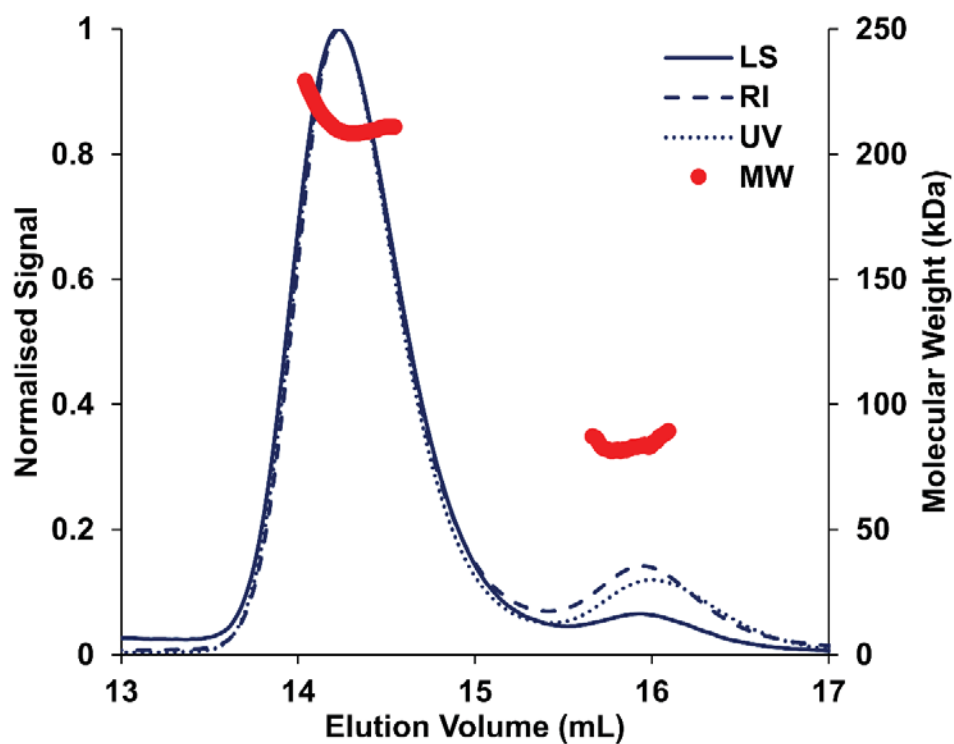


Figure 4: SEC-MALLS (size-exclusion chromatography with multi-angle laser light scattering) profile of Hyd-2-NOP in buffer containing detergent (Tris-HCl 20 mM, NaCl 150 mM, DTT 1 mM, DDM 0.02%, pH 7.2). The displayed molecular mass corresponds to the protein component of each peak alone (see methods). UV absorbance was measured at 280 nm. LS =laser scattering, RI =refractive index, MW =molecular mass.

The Structure of Hydrogenase-2 from *Escherichia coli*

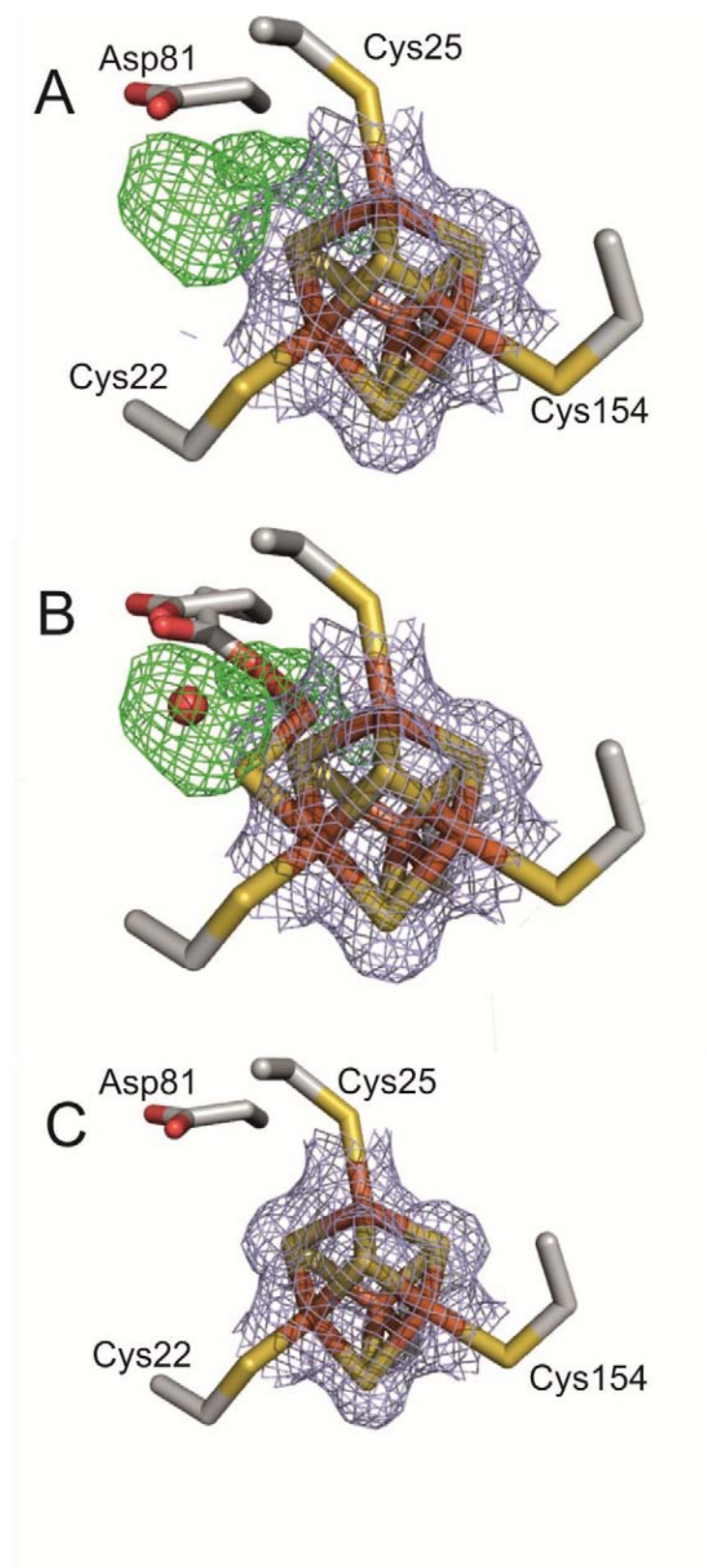


Figure 5: Structure of the proximal [4Fe-4S] cluster of HybO with 2Fo-Fc electron density shown as a grey mesh. **(A)** In as-isolated crystals modelling the cluster in a cubane conformation resulted in the appearance of additional Fo-Fc electron density peaks (green mesh) next to the cluster. These peaks were interpreted as an alternate conformation adopted by the cluster upon oxidative damage **(B)**, whereby the Fe atom coordinated by Cys25 moves away from the core of the cluster. Rotation of nearby Asp 81 allows the acidic group to coordinate the shifted Fe, and an additional water molecule (red sphere) occupies the remaining density next to the damaged cluster. **(C)** The proximal cluster and associated electron density for reduced Hyd-2 shows the cluster is in a single, cubane-like conformation with no uninterpreted Fo-Fc density.

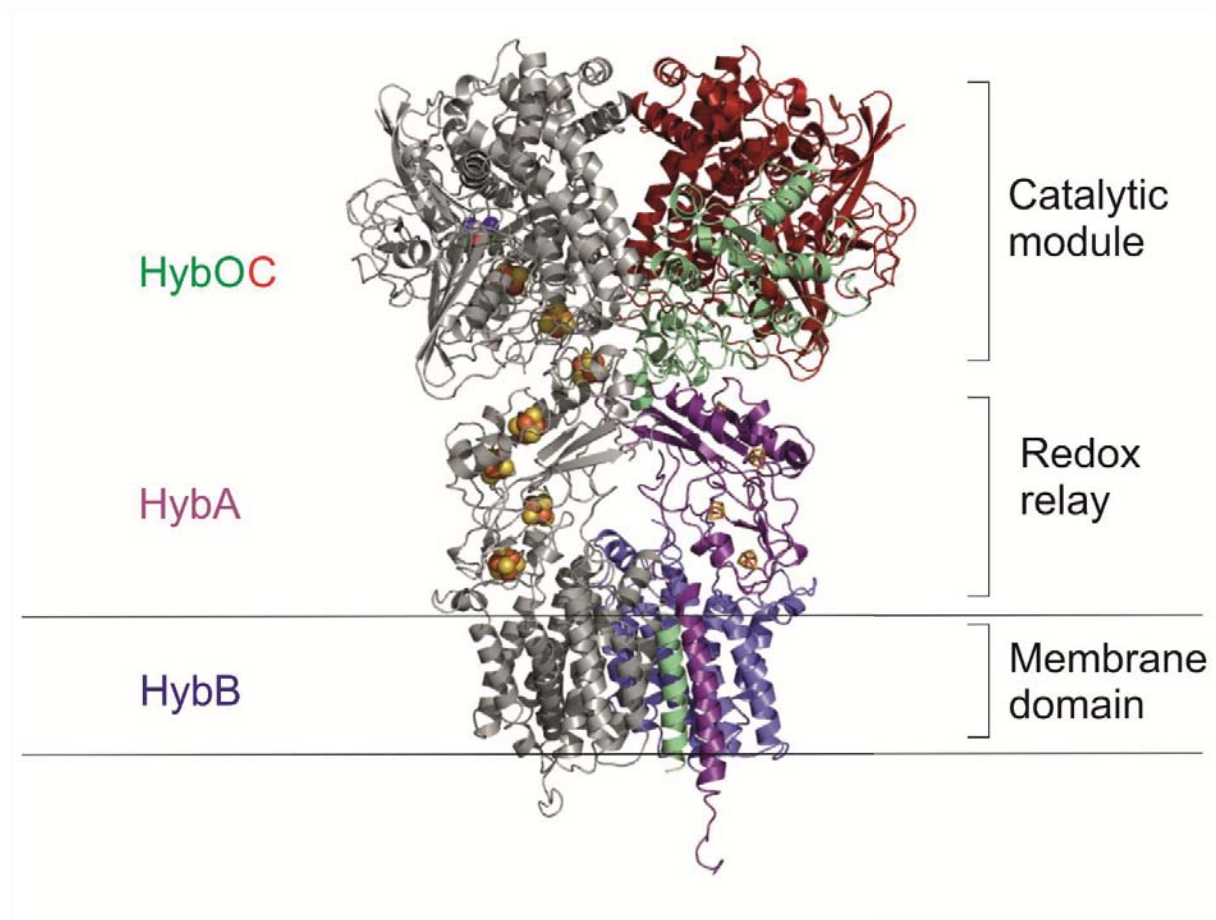
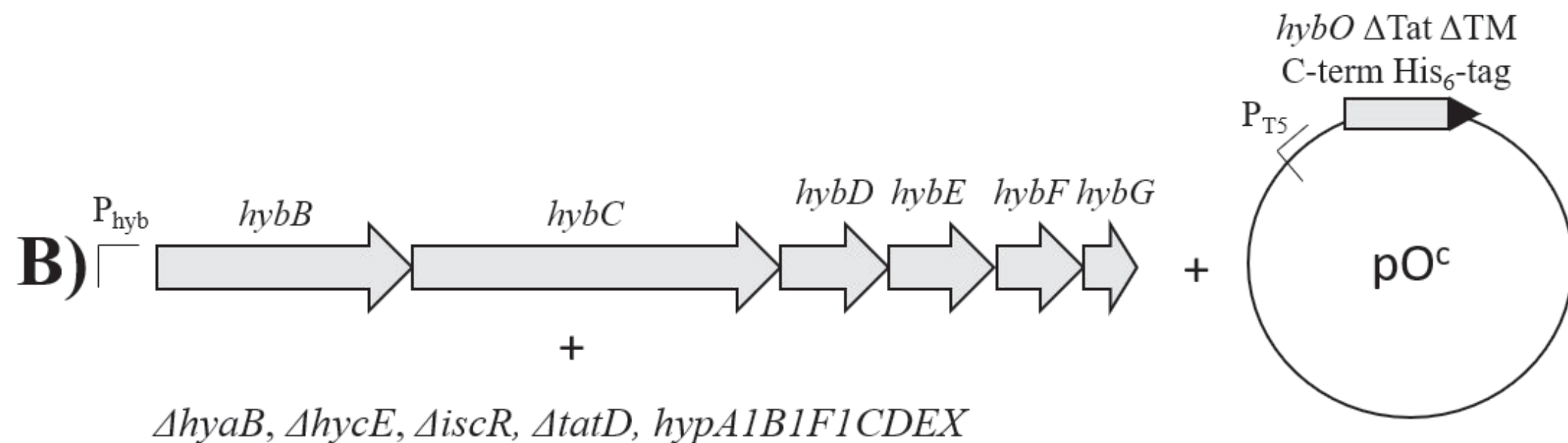
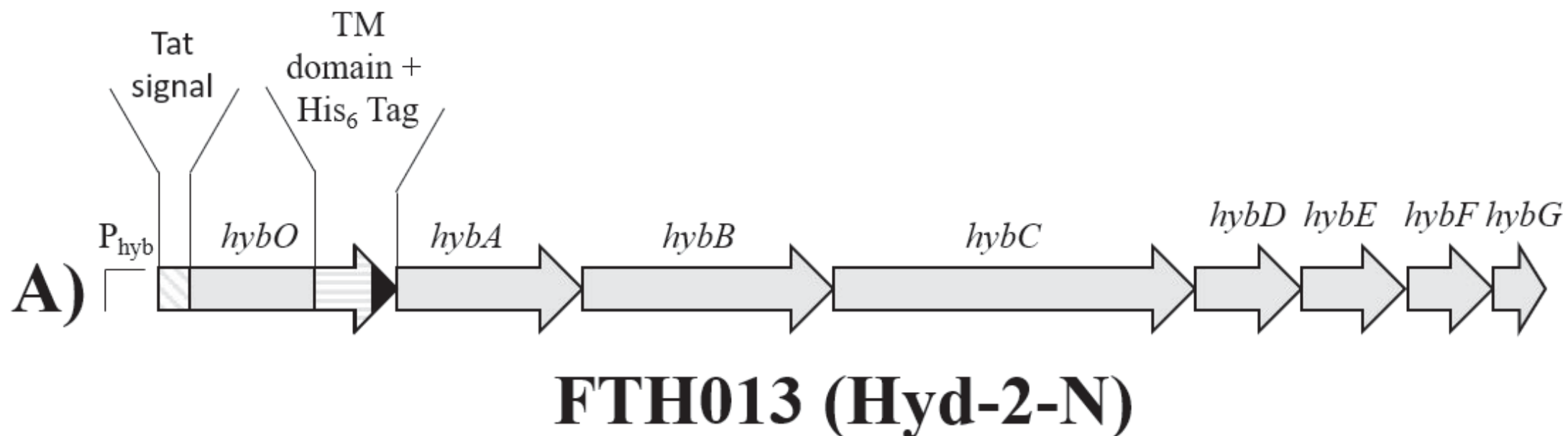
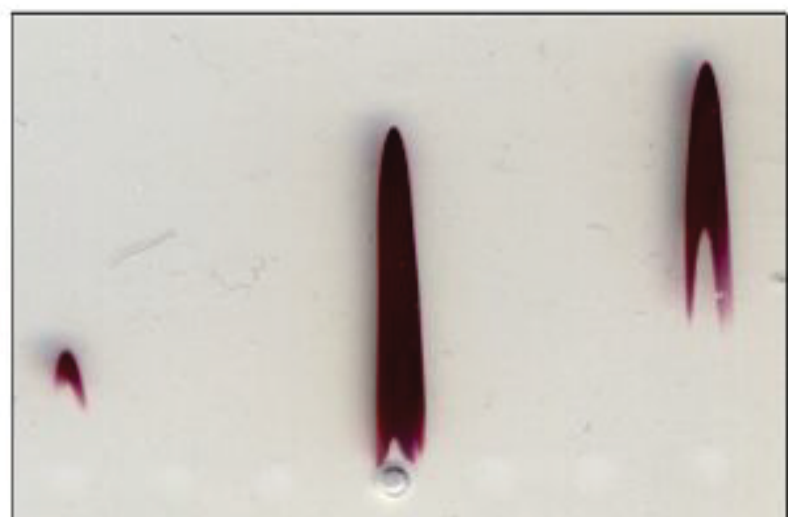


Figure 6: The crystal structure of $[\text{HybOC}]_2$ is combined with homology models of HybAB to show a proposal for the quaternary configuration of the membrane-bound $[\text{HybOCAB}]_2$ complex. The linker connecting the globular domain of HybO to the transmembrane helix has been omitted since its flexibility prohibits modelling its location with any degree of confidence.

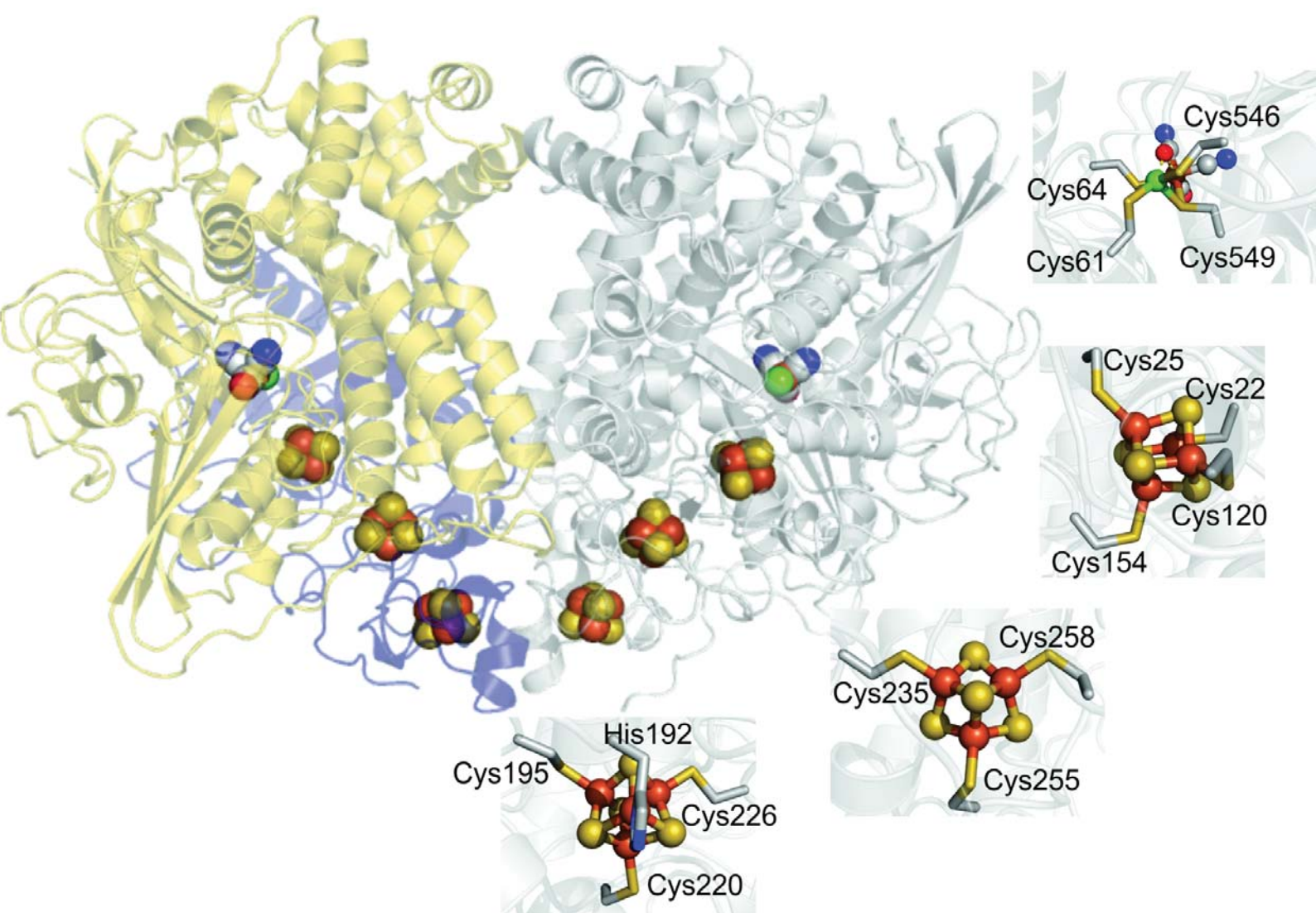


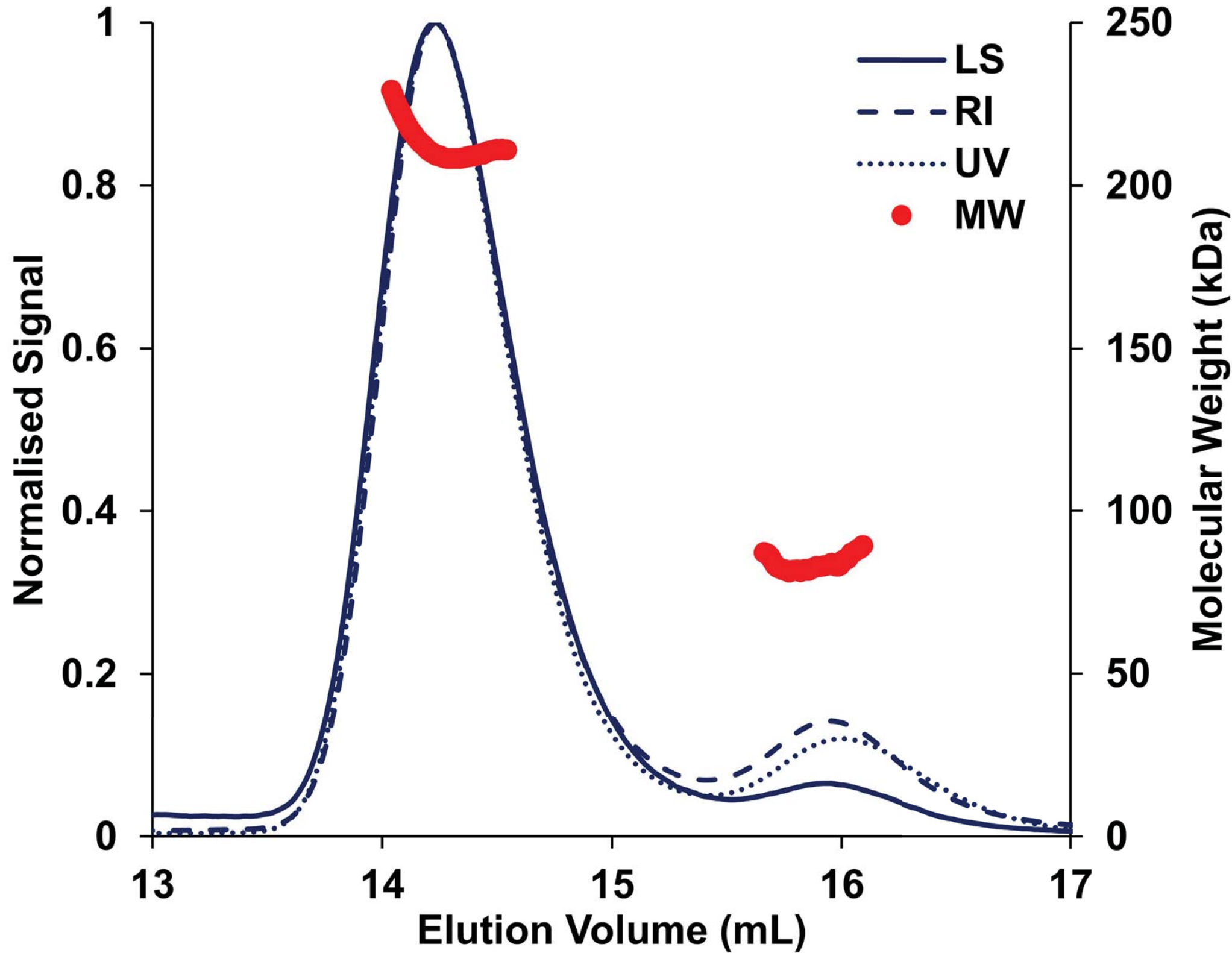
B

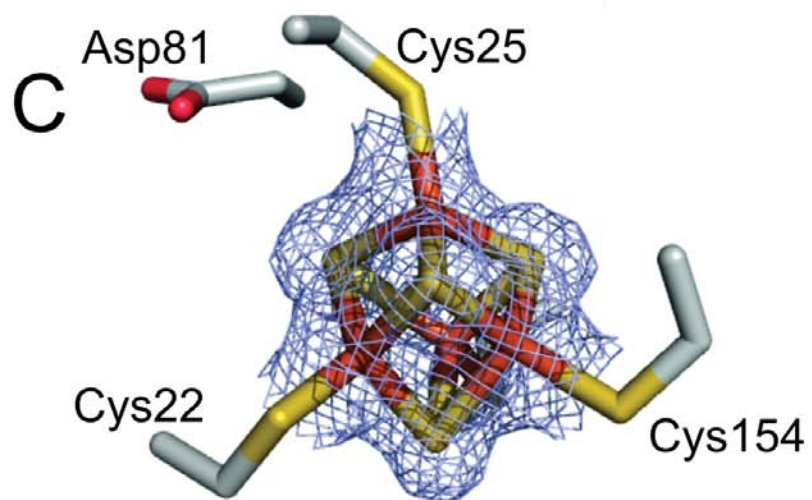
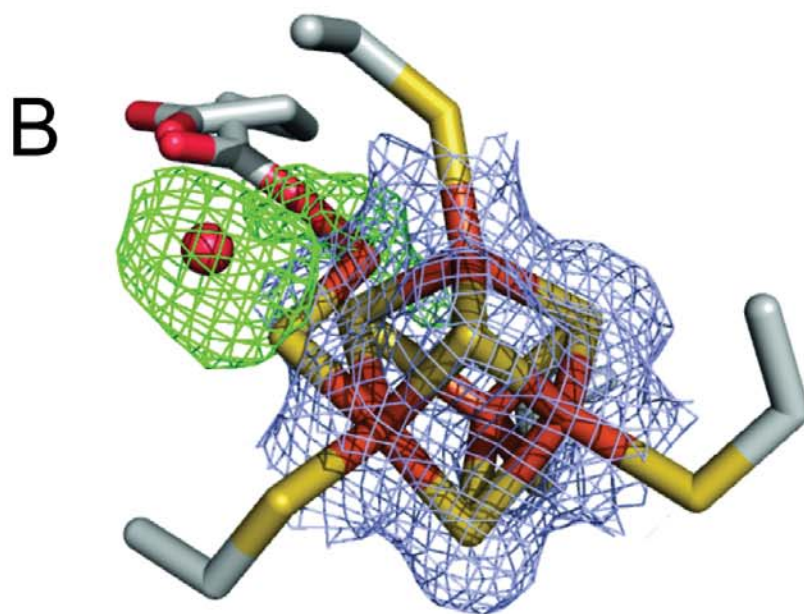
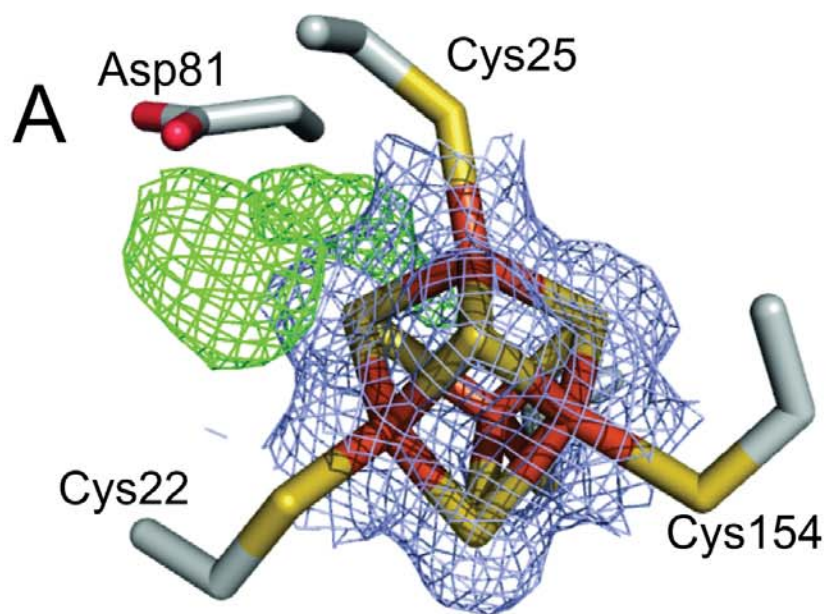

$$+ \frac{V_c \text{ pO}^N \text{ pO}^C}{\text{HJ001}} \frac{V_c \text{ pO}^N \text{ pO}^C}{\text{HJ001-hyp}}$$

$$\frac{\text{HJ001-hyp}}{V_c \quad pO^N \quad pO^C}$$









HybOC

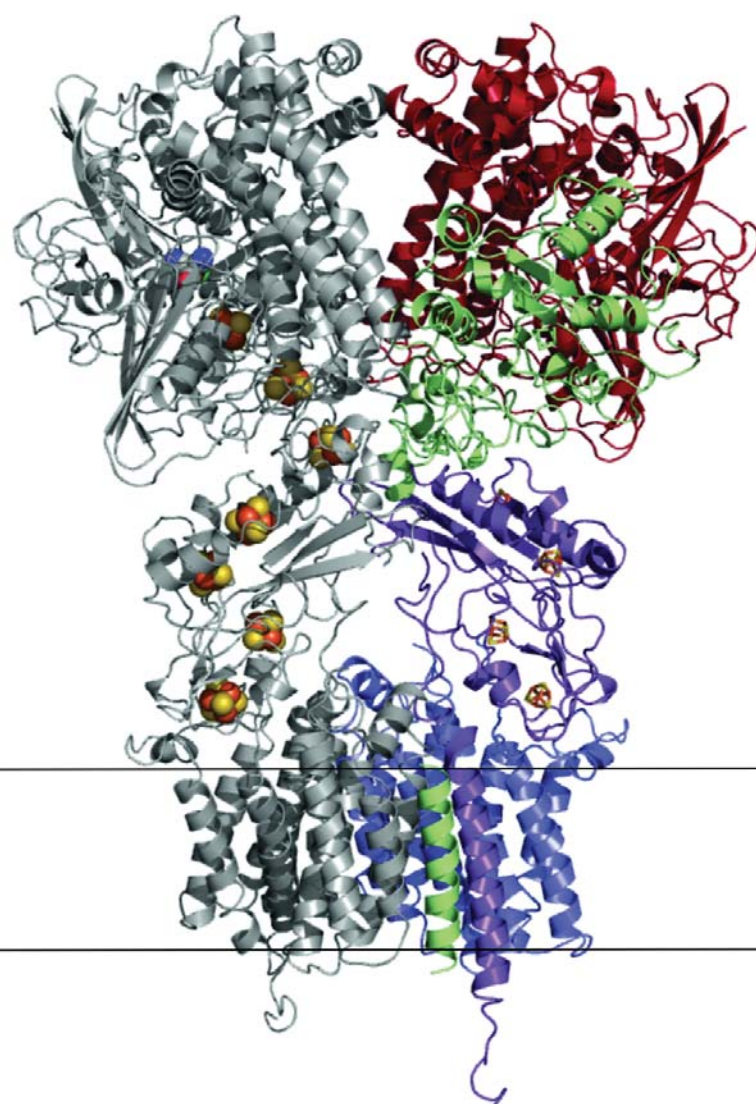
HybA

HybB

Catalytic
module

Redox
relay

Membrane
domain



The Structure of Hydrogenase-2 from *Escherichia coli* and a Draft Quaternary Complex for H₂-driven Proton Pumping

Stephen E. Beaton¹, Rhiannon M. Evans¹, Alexander J. Finney², Ciaran M. Lamont²,

Fraser A. Armstrong^{1*}, Frank Sargent^{2*} and Stephen B. Carr^{3,4*}

¹Department of Chemistry, Inorganic Chemistry Laboratory, University of Oxford, Oxford OX1 3QR. ²Division of Molecular Microbiology, School of Life Sciences, University of Dundee, Dundee DD1 5EH, UK. ³Research Complex at Harwell, Rutherford Appleton Laboratory, Harwell Oxford, Didcot OX11 0FA, UK, ⁴Department of Biochemistry, University of Oxford, Oxford OX1 3QU, UK.

*Correspondence: fraser.armstrong@chem.ox.ac.uk; f.sargent@dundee.ac.uk; stephen.carr@rc-harwell.ac.uk

Supplementary Information

Contents

Figure S1 – Graphic representation of the function and arrangement of Hyd-2 subunits

Table S1 – Strains, oligonucleotide primers, and plasmid constructs used in this study

Figure S2 – SDS-PAGE analysis of Hyd-2-NOP during purification for structural determination

Figure S3 – Comparison of Michaelis constant of H₂ for Hyd-2 and Hyd-2-NOP

Figure S4 – Comparison of enthalpy of activation for Hyd-2-N and Hyd-2-NOP

Figure S5 – Comparison of activation profile (E_{switch}) of Hyd-2-N and Hyd-2-NOP

Figure S6 – Comparison of product inhibition for Hyd-2-N and Hyd-2-NOP

Figure S7 – EPR spectra of reduced and oxidized Hyd-2-NOP at 80K and 15K

Figure S8 – Structural differences between Hyd-2 and Hyd-1

Figure S9 – SDS-PAGE analysis of dissolved Hyd-2 crystals

Figure S10 – Active site overlay of Hyd-1 and Hyd-2

Figure S11— Comparison of the active sites in hydrogen reduced Hyd-2

Figure S12 – Hyd-2 FeS cluster distances

Figure S13 – Sequence alignment of selected [NiFe(Se)]-hydrogenases

Figure S14 – Map of hydrophobic patches on the surface of Hyd-2

Graphic representation of the function and arrangement of Hyd-2 subunits

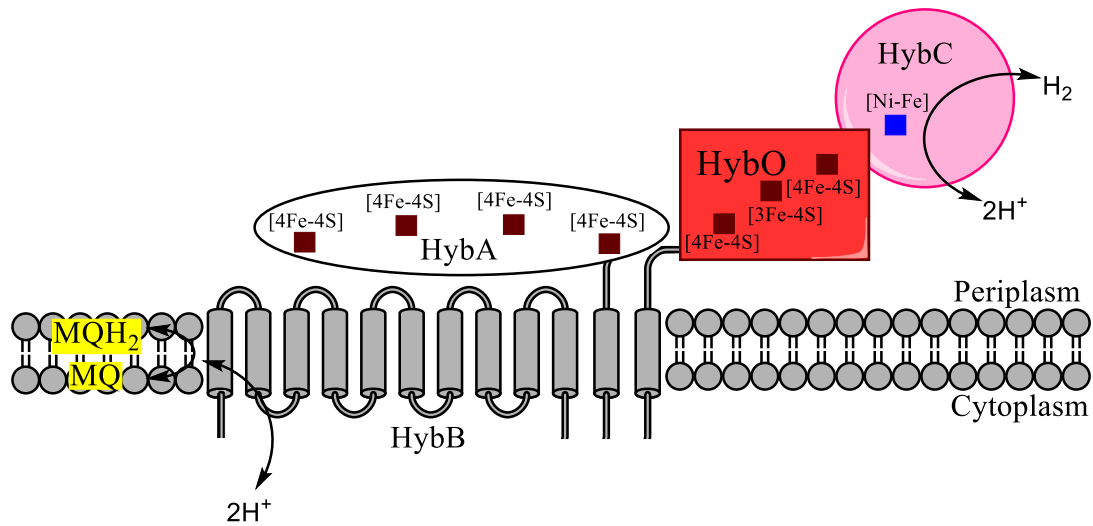


Figure S1: Minimal schematic of the position of different subunits of Hyd-2 in relation to the periplasmic membrane illustrating the reduction and oxidation occurring in the quinone pool at HybB and a pathway for electron relay through the FeS clusters HybA and HybO to the NiFe cofactor of HybC.

Table S1: Strains, oligonucleotide primers, and plasmid constructs used in this work.

Strain	Genotype	Purpose	Source
MC4100	F ⁻ , Δ lacU169, <i>araD139</i> , <i>rpsL150</i> , <i>relA1</i> , <i>ptsF</i> , <i>rbsR</i> , <i>flbB5301</i>	Parent strain for construction of IC011	¹
IC011	As MC4100, Δ <i>hyaB</i> , Δ <i>hycE</i> , Δ <i>hybOA</i>	Parent strain for construction of HJ001	²
HJ001	As IC011, Δ <i>iscR</i>	Parent strain for construction of HJ001-hyp	²
HJ001-hyp	As HJ001, Δ <i>tatD::hypA1-X</i>	Used for production of Hyd-2-NOP	This work
FTH013	As MC4100, with C-terminal hexa-his tag on <i>hybO</i>	Used for production of Hyd-2-N	³
FTD674	chromosomal in frame deletion between <i>hybO</i> codons 328 (encoding glutamate) and 355 (encoding valine) thus removing a hydrophobic region predicted to form a TM	Positive control strain for Rocket immunoelectrophoresis, produces a soluble form of Hyd-2	⁴
Primer Name	Primer Function	Primer Sequence	Source
hybO_F	Amplify Δ TAT Δ TM <i>hybO</i> forwards primer with pQE-80L overlap	5'-GAATTCGAGCTCGCGGCCGCACTAG TCACAGAGGAACAGGTATGGAGATGGCCGA ATCGGTTACTAACC-3'	This Work
hybO_R	Amplify Δ TAT Δ TM <i>hybO</i> reverse primer with pQE-80L overlap	5'-GTCGACGCGGCCGCCCTAGGTTA TTAGTGATGGTGATGGTGATGGCC GCCCTCTTTAGCGTTAACATCC-3'	This Work
OpenpQE80_F	Amplify linear pQE-80L construct forwards primer	5'-CCTAGGGCGGCCGCGTCGACCTGCA GCCAAGCTTAATTAGCTGAGC-3'	This Work
OpenpQE80_R	Amplify linear pQE-80L construct reverse primer	5'-ACCTGTTCTCTGTGACTAGTGCGGC CGCGAGCTCGAATTCTGTGTGAAA TTGTTATCCGCTCACAATTG-3'	This Work

Plasmid	Identifier	Purpose	Source
pQE-80L	Vc	Vector used for cloning of N- or C-terminal his-tagged, <i>hybO</i> Δ TAT Δ TM	Qiagen
pQE-80L <i>hybO</i> Δ TAT Δ TM C-terminal hexa-his tag	pO ^C	Used for overproduction of soluble <i>hybO</i> with C-terminal hexa-his tag	This work
pQE-80L <i>hybO</i> Δ TAT Δ TM N-terminal hexa-his tag	pO ^N	Used for overproduction of soluble <i>HybO</i> with N-terminal hexa-his tag	This work
pFAT122		pBluescript II KS(+)-based vector containing 551 bp fragment covering the downstream region and last two codons of <i>tatD</i> as an EcoRI/Sall fragment	⁵
pFAT123		pFAT122, also containing 557 bp fragment covering the upstream region and first two codons of <i>tatD</i> as a Sall/KpnI fragment.	⁵
pBluescript Δ <i>tatD</i> :: <i>hypA1-X</i>		Contains Δ <i>tatD</i> :: <i>hypA1-X</i> allele as XbaI/KpnI fragment	This work
pMAK705 Δ TAT:: <i>hybA1-X</i>		Contains Δ <i>tatD</i> :: <i>hypA1-X</i> allele, for transfer to to chromosome of strain HJ001, creatinf strain HJ001-hyp	This work

Denaturing electrophoresis of Hyd-2-NOP

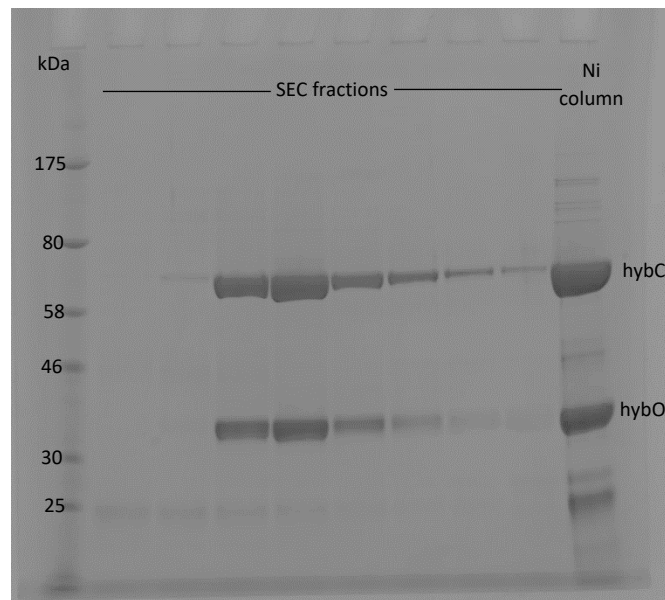


Figure S2: SDS-PAGE analysis of purified Hyd-2-NOP; after purification by Ni-affinity chromatography, Hyd-2-NOP-containing fractions were pooled, concentrated, and dialyzed into a buffer containing DDM, then further purified by size-exclusion chromatography (SEC). Fractions of the elution from SEC are shown as well as the concentrated sample that has only undergone Ni-affinity chromatography.

Comparison of Michaelis constant of H_2 for Hyd-2 and Hyd-2-NOP

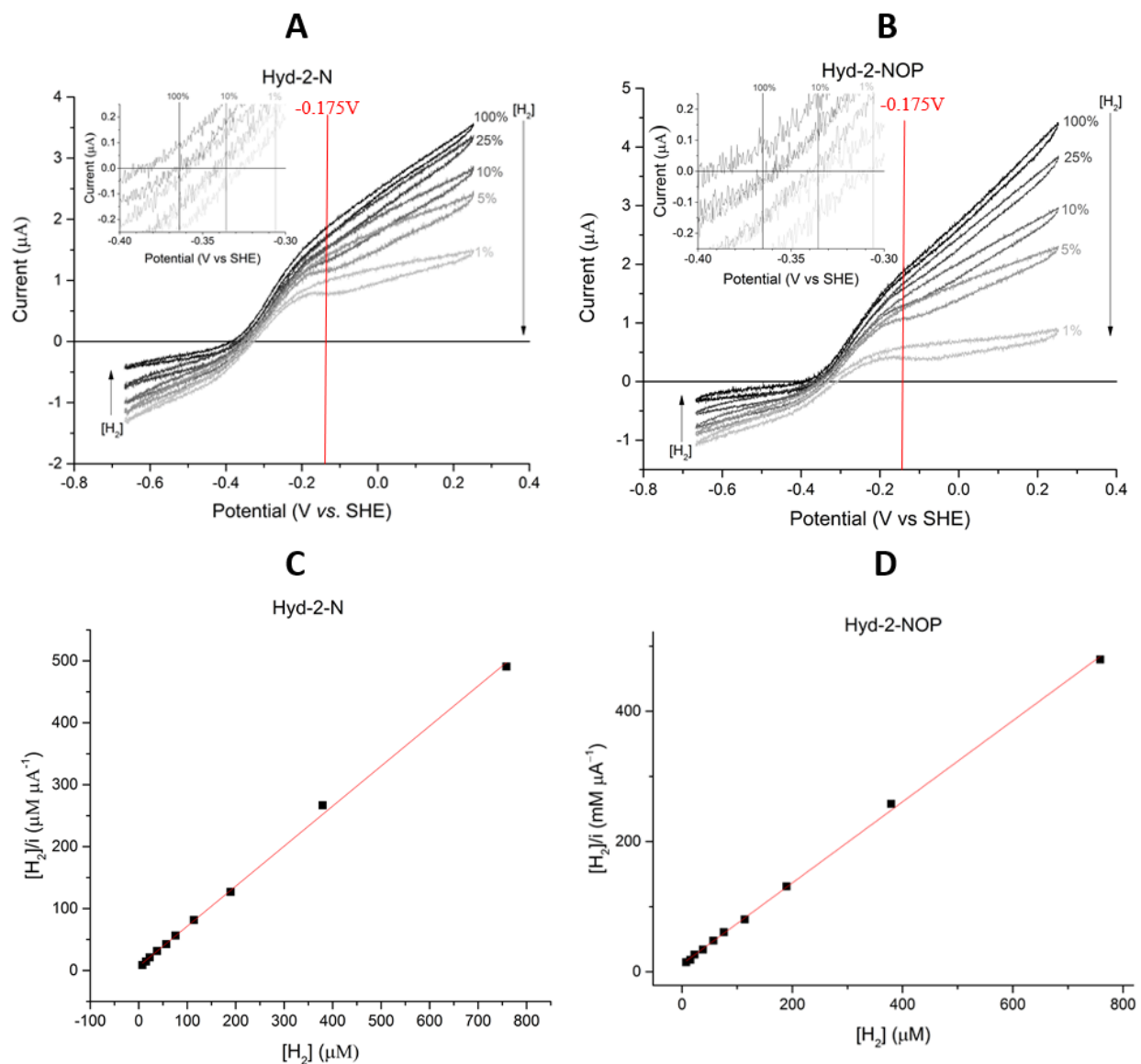


Figure S3: Measurements of K_M for Hyd-2-N (panels A and C) and Hyd-2-NOP (panels B and D). Cyclic voltammograms at 5 mV/s (A and B) were measured at 10 different H_2 concentrations, returning to 100% H_2 every three scans to account for film loss (for clarity only four H_2 concentrations are shown). The zero-current potential corresponds well to the values predicted by the Nernst equation (A and B insets). The calculated K_M is derived from a Hanes-Woolf plot (C and D) using data across the entire $[H_2]$ range and is reported at -0.175 V (Table 1) for comparison to previously published data.

Comparison of enthalpy of activation for Hyd-2-N and Hyd-2-NOP

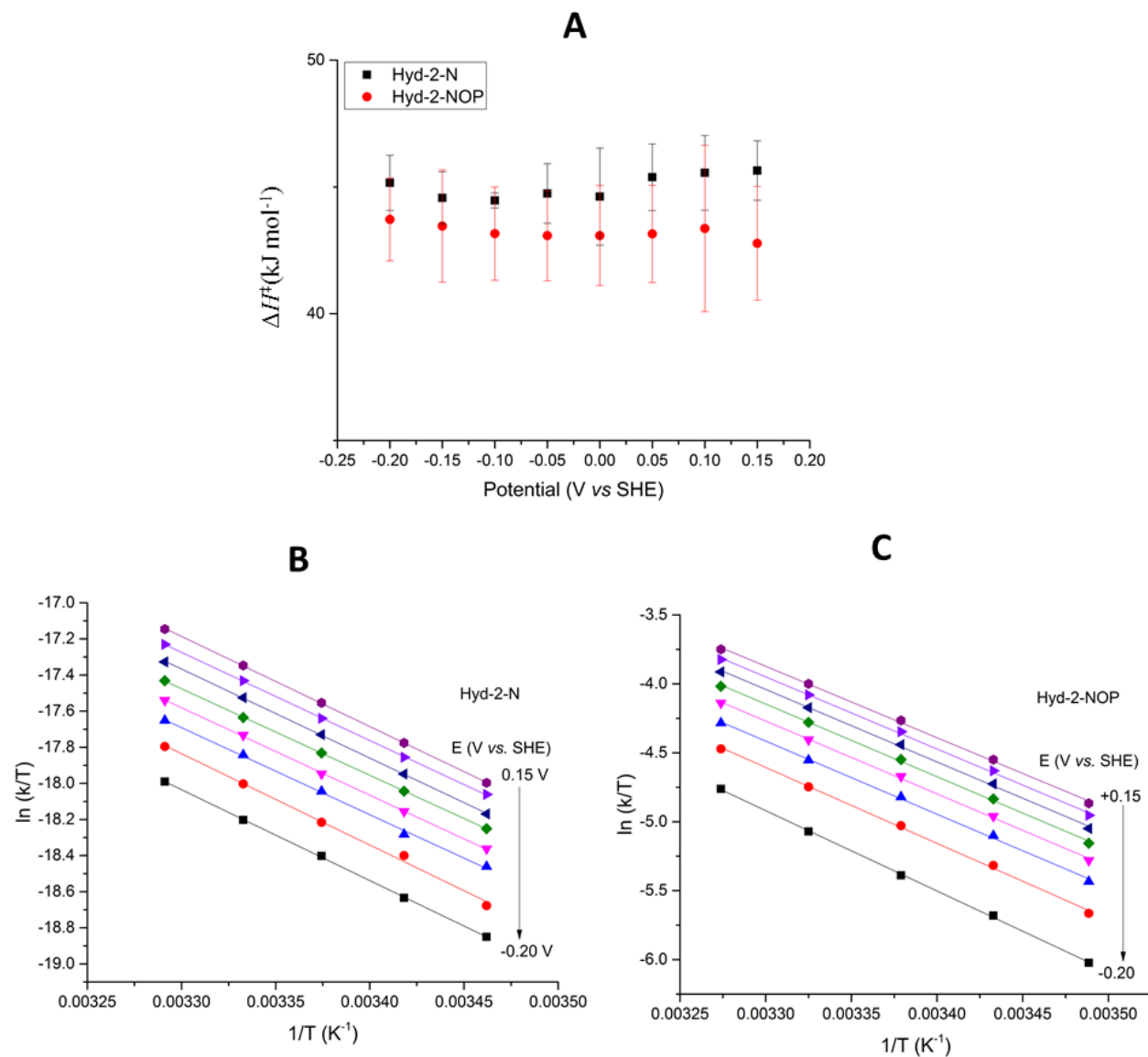


Figure S4: Hydrogen oxidation activity (-0.200 V vs. SHE) at varying temperatures is analyzed with Eyring plots (panels B and C) to reveal similar enthalpies of activation (see Table 1) for Hyd-2-N and Hyd-2-NOP (panel A).

Comparison of activation profile (E_{switch}) of Hyd-2-N and Hyd-2-NOP

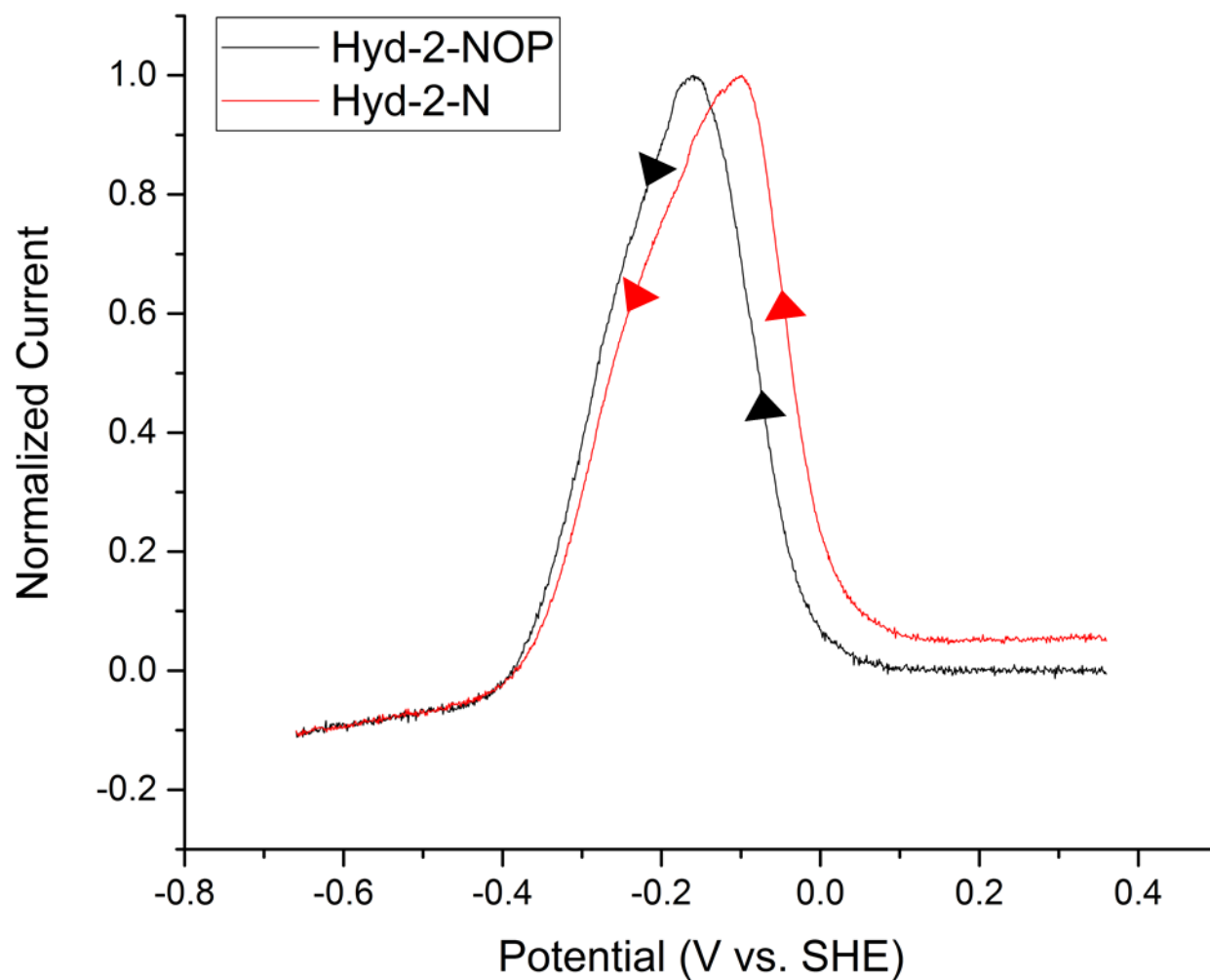


Figure S5: Overlay of backwards scans following anaerobic inactivation at high potential. The driving force required to reactivate Ni-B gives insight into the stability of the resting inactive state. Data have been normalized to max current for each experiment for easier comparison. The variance between Hyd-2-N and Hyd-2-NOP is within error of each other.

Comparison of product inhibition for Hyd-2-N and Hyd-2-NOP

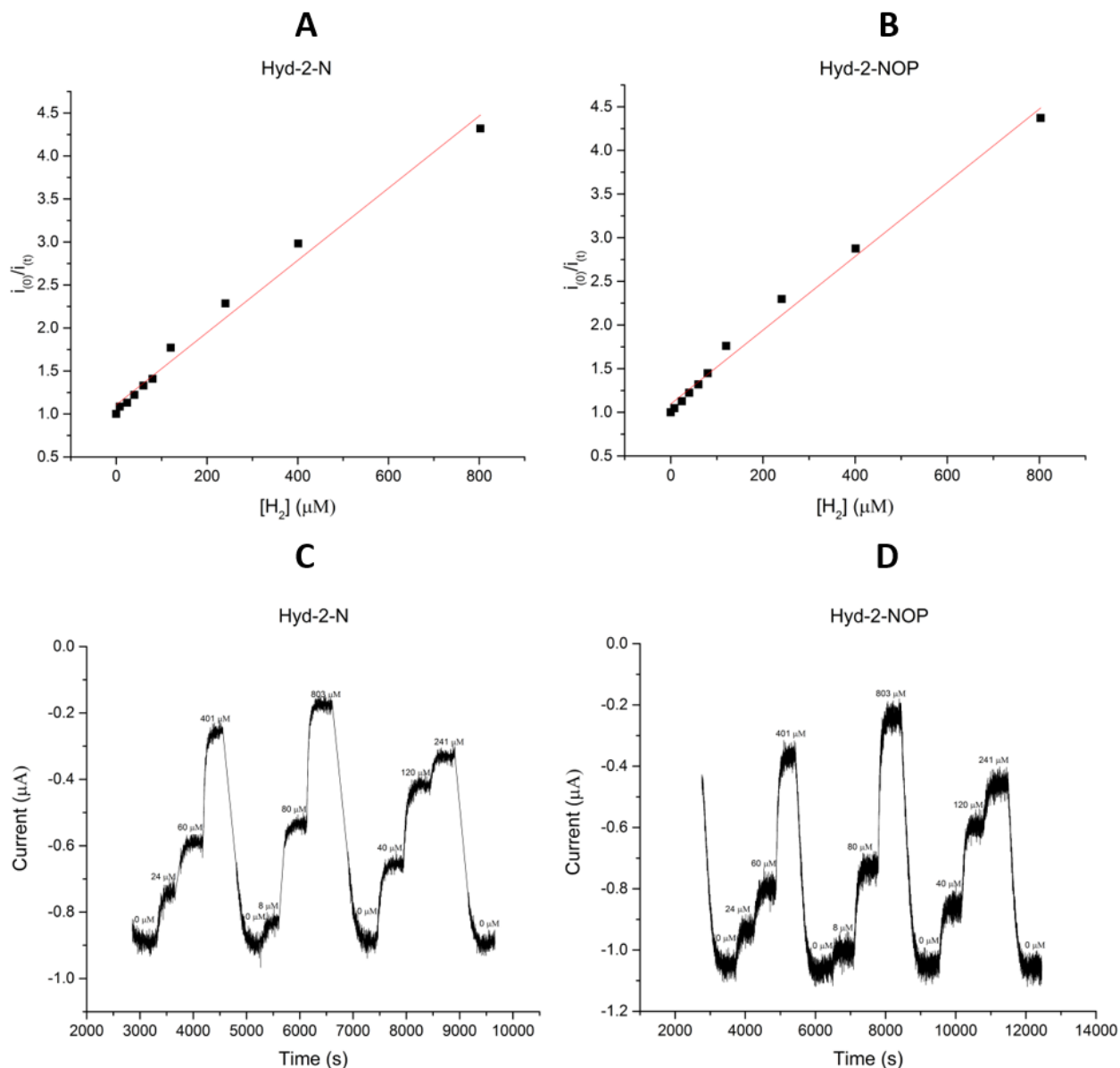


Figure S6: Comparison of H_2 production activity with varying concentration of H_2 at -0.175 V vs. SHE between Hyd-2-N (panels A and C) and Hyd-2-NOP (panels B and D). The effect of product inhibition on current (panels C and D) is nearly identical for both enzymes and the inhibition constant is calculated (see Table 1) as the inverse slope when plotting the ratio of the uninhibited current ($i_{(0)}$) to inhibited current ($i_{(t)}$) against the concentration of H_2 (panels A and B).

EPR spectra of reduced and oxidized Hyd-2-NOP at 80K and 15K

Continuous wave measurements were carried out using an X-band (9.1-9.9 GHz) Bruker EMX spectrometer equipped with a low temperature helium flow cryostat (Oxford Instruments CF935).

The EPR samples were prepared using as-isolated enzyme in MES buffer (100 mM MES, 100 mM NaCl, 10% glycerol, pH 6) with added mediators (40 μ M each, 1,2-napthoquinone, phenazinemethosulfate, indigo tetrasulfonate, 2-hydroxy-1,4-napthoquinone, benzyl viologen, methyl viologen). In an anaerobic glovebox (Belle Technologies, O₂ <2 ppm), the enzyme was stirred in a gas tight cell at 20 °C under an atmosphere of Ar. The potential of the solution was monitored using a two-electrode system which comprised a Pt working and Ag/AgCl reference electrode. Small aliquots of Na₂S₂O₄ (200 mM and 400 mM diluted in pH8 borate buffer) and K₃[Fe(CN)₆] (200 mM and 400 mM diluted in MES buffer) were added whilst continuously monitoring the potential of the sample. The as-isolated enzyme was first oxidized (+380 mV, data not shown) before being reduced to a mildly oxidizing potential (+150 mV) and finally a fully reducing potential (−230 mV). Enzyme samples were taken as 250 μ L aliquots, transferred from the cell to EPR tube (W707-SQ-250, 4 mm low precision, Fluorochem) with a gas tight syringe and flash frozen in an isopropanol slush.

EPR spectrum of reduced and oxidized Hyd-2-NOP at 80K and 15K

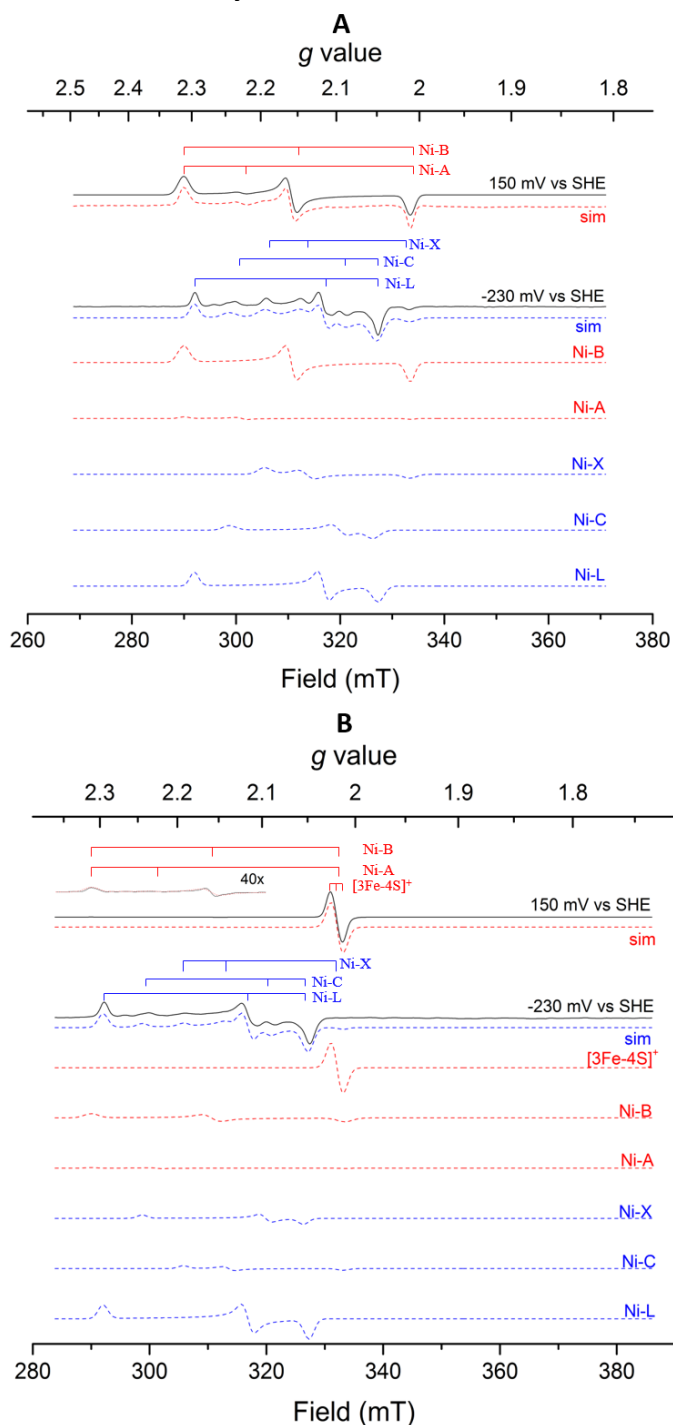


Figure S7: X-band continuous wave EPR measurements of Hyd-2-NOP at 80K (A) and 15K (B). Microwave power 2.00 mW; modulation amplitude 1.0 mT. Protein concentration was ~25 μ M. Ni-A: $g_x = 2.309$, $g_y = 2.225$, $g_z = 2.009$; Ni-B: $g_x = 2.309$, $g_y = 2.157$, $g_z = 2.009$; [3Fe-4S]⁺: $g_x = 2.02$, $g_y = 2.017$, $g_z = 2.015$; Ni-X: $g_x = 2.242$, $g_y = 2.095$, $g_z = 2.053$; Ni-C: $g_x = 2.193$, $g_y = 2.137$, $g_z = 2.01$; Ni-L: $g_x = 2.293$, $g_y = 2.115$, $g_z = 2.047$. Spectra simulation generated using Hyperfine Spectrum (WR Hagen Visual Software).

Structural differences between Hyd-2 and Hyd-1

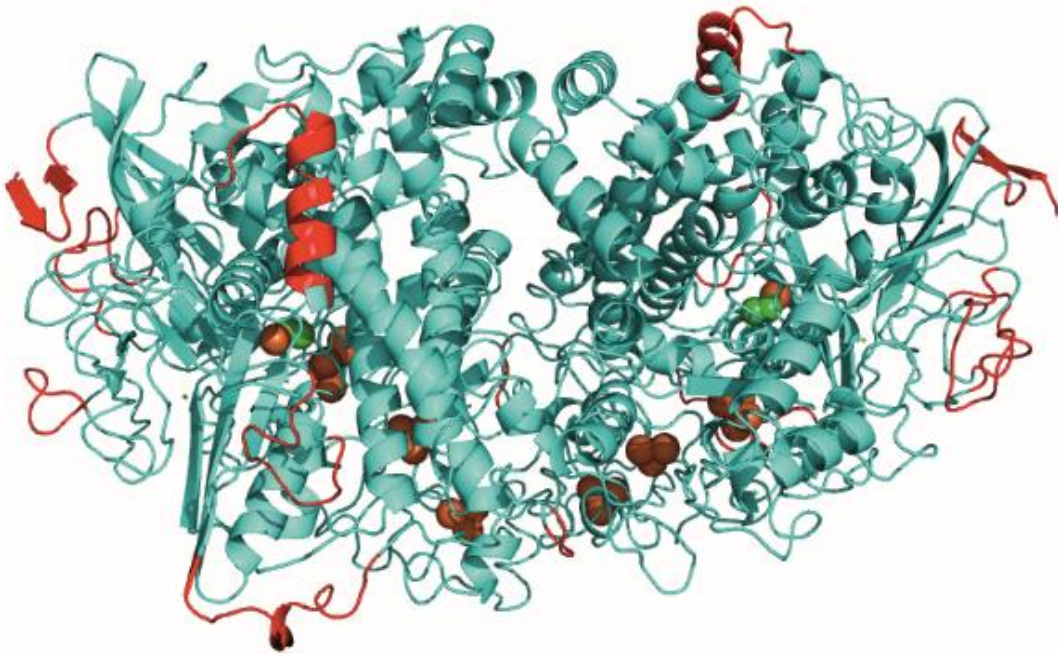


Figure S8: Comparison of the structures of *E. coli* hydrogenases Hyd-1 and Hyd-2. Superposition (using secondary structure motifs) shows the polypeptide backbones overlay well with a calculated r.m.s.d. of 1.2 Å. The largest differences in structure are located at the surface of the protein and result from elongation of surface loops in Hyd-1 relative to Hyd-2. The structure shown is Hyd-1 with any major points of difference with Hyd-2 highlighted in red.

SDS-PAGE analysis of dissolved Hyd2 crystals.

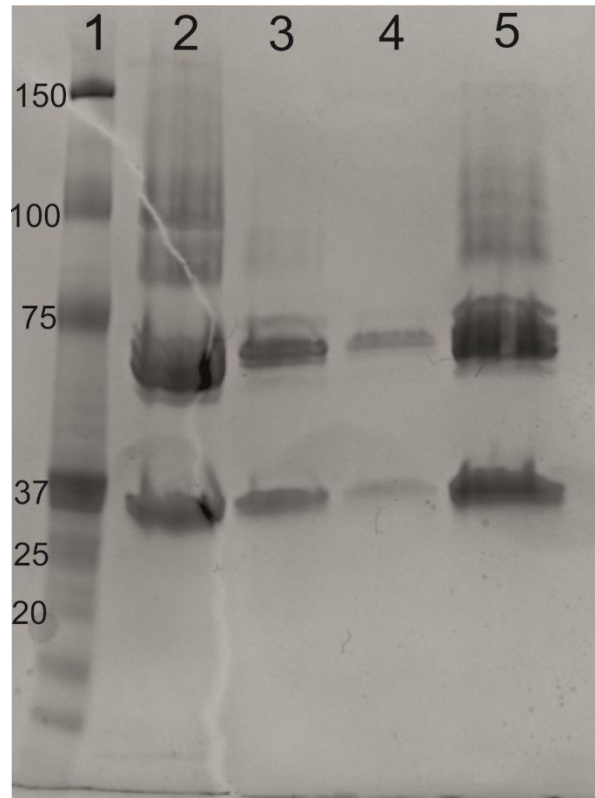


Figure S9: Approximately 20 crystals of Hyd-2-NOP were looped and washed in crystallization buffer before being dissolved in water. Dissolved crystals were mixed with 20 μ L Ni sepharose beads pre-equilibrated with 20 mM tris pH 7.2, 350 mM NaCl, 60 mM Imidazole. The beads were washed twice with the same buffer before protein was eluted with 20 mM tris pH 7.2, 350 mM NaCl, 500 mM Imidazole. Fractions from each step were analysed by SDS-PAGE. Lane 1 = protein marker, lane 2 = Protein loaded, lane 3 = first wash, lane 4 = second wash, lane 5 = eluted protein. Both protein subunits (HybC and HybO) are visible in the load/elution lanes in approximately equal quantities. The protein derived from crystals retains the ability to bind to Ni-chelating resin showing that the His-tag is intact. Since the tag is at the C-terminus of the small subunit the unstructured linker (residues 273-299) that is not visible in the electron density must also be present in the crystals.

Active site overlay of Hyd-1 and Hyd-2

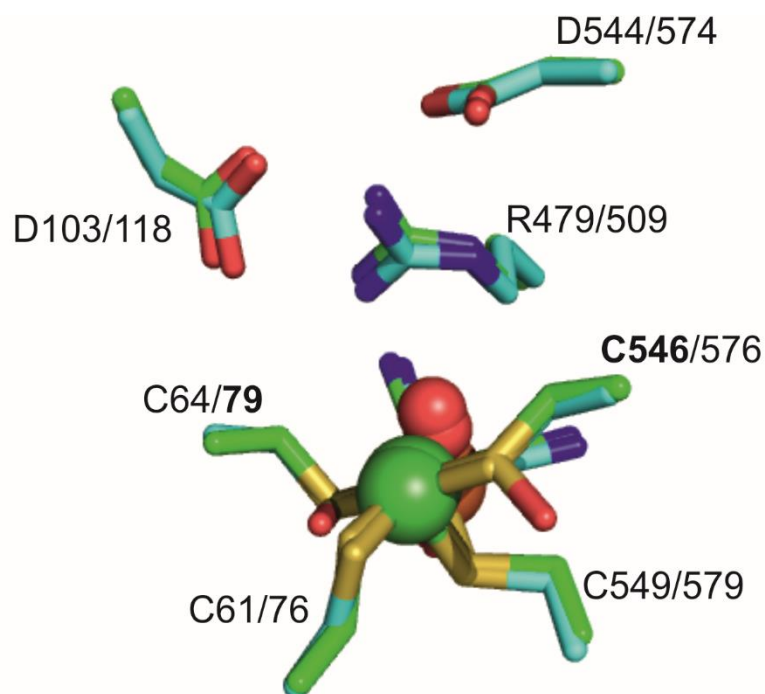


Figure S10: Overlay of the active site 'Canopy' region of Hyd-2 (green) and Hyd-1 (cyan). The overall fold and positioning of residues in the canopy is unchanged between the two enzymes. Oxidative damage at the active site in the form of oxidation of metal coordinating cysteine residues is observed at the NiFe cluster and could contribute to the formation of an inactive unready (Ni-A) state that is difficult to reductively reactivate. In Hyd-2 C546 becomes oxidized upon prolonged exposure to air, whereas in Hyd-1 the oxidative damage occurs at C79 (both indicated in bold). Each residues is identified with Hyd-2-numbering shown first.

Comparison of active site sites in hydrogen reduced Hyd-2

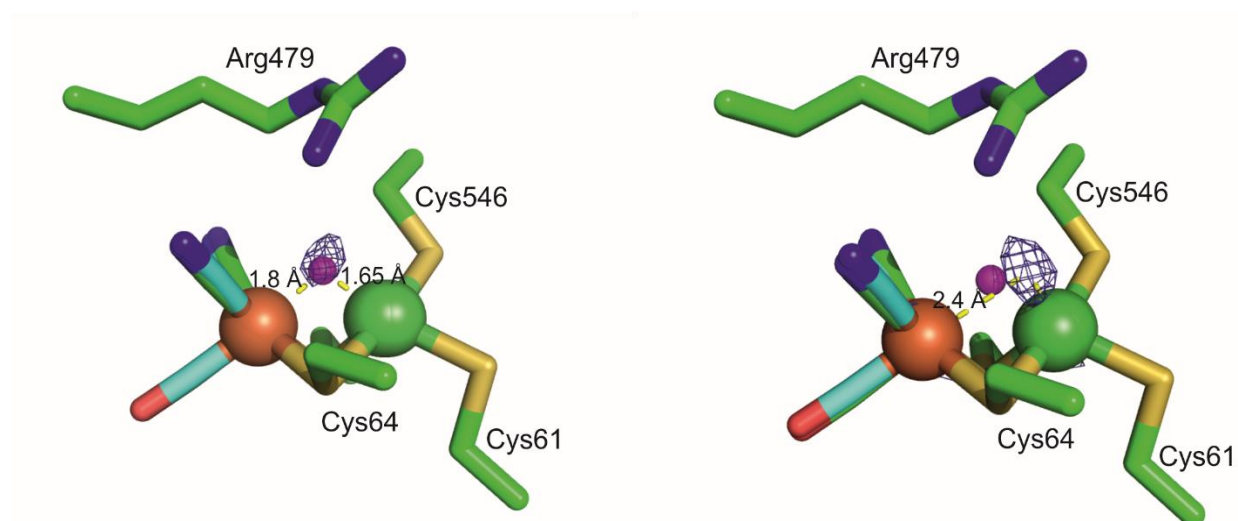


Figure S11: The active sites in each heterodimer of as-isolated Hyd-2 appear identical, however, after hydrogen reduction the location of the electron density peak in the bridging position clearly differs in the active sites in each of the two hybC subunits. In chain L (left) the peak is more central and superposition of the Ni-R active site from *D. vulgaris* Miyazaki F (cyan) and Hyd-2 (green) places the bridging hydride within a peak of Fo-Fc difference density suggesting the active site of Hyd-2 is also in the Ni-R state. The active site of the second HybOC dimer (chain M, right) Fo-Fc density is also observed between the metals, but it has shifted towards the Ni atom such that its centroid is 2.45 Å from the Fe and 1.6 from the Ni. Superposition of the Ni-R active site no longer places the hydride in the electron density implying this may represent another intermediate of the catalytic cycle.

Hyd-2 FeS cluster distances

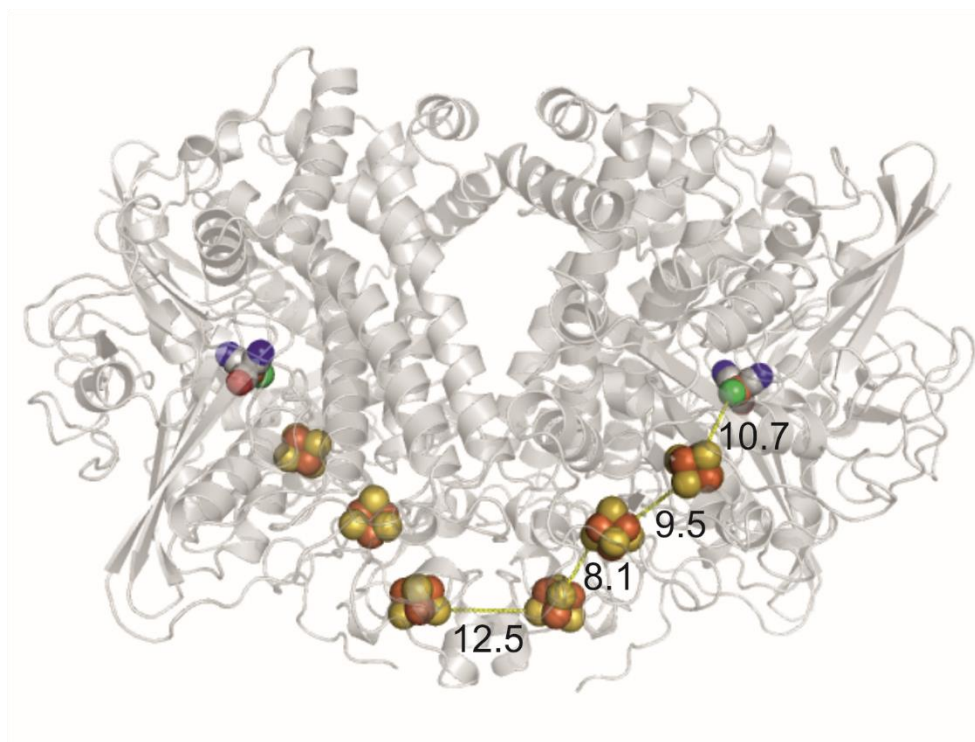


Figure S12: Location of the metal clusters in Hyd-2 with distances between the closest atoms between each FeS cluster and active site Ni atom shown in Angstroms. The distance between the distal clusters of each heterodimer is 12.5 Å, a distance that is typical of all other $\alpha_2\beta_2$ hydrogenases crystalized to date and is well below the average distance required for efficient electron tunneling.⁶

Sequence alignment of selected [NiFe(Se)]-hydrogenases

		81
<i>E. coli</i> Hyd2 (1c)	→→	NALEKYKGQYVLVVDGSIPLKDN---GIYCMVAG-----EPIVDHIRKAAEGAAA
<i>A. vinosum</i> (1e)	→→	QAMDENRGQYLIVIVDGSIPGPDAN--PGFSTVAG-----HSNYSILMETVEHAAA
<i>D. fructosovorans</i> (1b)	→→	QALEGKDG-YLLVVEGGLPTIDG---GQWGMVAG-----HPMIETTKAAAKAKG
<i>D. gigas</i> (1b)	→→	EAIKG--D-FVCVIEGGIPMGDG---GYWGVGR-----RNMYDICA EVAPKAKA
<i>D. vulgaris</i> MF (1a)	→→	QAVNSPHG-FIAVVEGGIPTAAN---GIYKVAN-----HTMLDICSRLPKAQA
<i>R. eutropha</i> Actinobacterial-type (1h)	→→	KAARGEIDN FVLVLEGGIPNERINGEGYWAAMGT---DPQTHQPITIP EWLDR LAPKALA
<i>E. coli</i> Hyd-1 (1d)	→→	DIITQYNGKYILAVEGNPPLGEQ---GMFCISSG-----RPFIEKLKRAAGASA
<i>S. typhimurium</i> Hyd5 (1d)	→→	DVMREYKGN YIVAVEGNAPLNED---GMFCILAG-----EPFLEKLKRV SADAKA
<i>H. marinus</i> (1d)	→→	EIKEKYKGN YILAVEGNPPLNQD---GMSCIIGG-----RPFSEQLKRMADDAKA
<i>R. eutropha</i> MBH (1d)	→→	EIMTKYKGN YILAVEGNPPLNQD---GMSCIIGG-----RPFIEQLKYVAKDAKA
<i>A. aeolicus</i> (1d)	→→	RIIKEYWGN YILAVEGNPPLGED---GMYCIIGG-----RPFVEILKESAEGAKA
<i>D. baculatum</i> NiFeSe (1a)	→→	EIAEKFN GNFFLLVEGA IPTAKE---GRYCIVGETLDAKAHHHEVTMMELIRDLAPKSLA
<i>D. vulgaris</i> Hborough NiFeSe (1a)	→→	KVAEKFKGKFLLVIEG SVPEAD---GKYCIIGE----ANHHEISMVDALKEFGPNAAA
		. : : * *

Figure S13: Sequence alignment (Clustal Omega) of the small subunits of selected [NiFe]-hydrogenases, highlighting the conservation of D81 at the equivalent position. The subgroup to which each hydrogenase is categorized is given in parentheses. Asterisks represent amino acids that are strictly conserved, a colon represents amino acids that are highly conserved, and a period represents amino acids that are weakly conserved.

Map of hydrophobic patches on the surface of Hyd-2

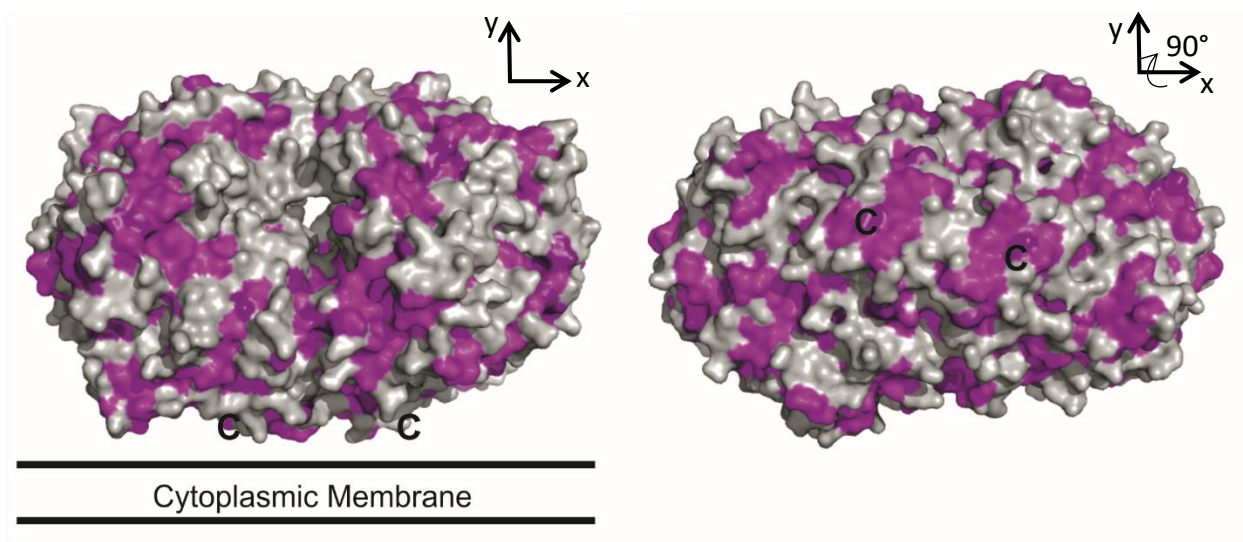


Figure S14: Distribution of hydrophobic residues across the surface of the [HybOC]₂ catalytic core. Obvious symmetrical patches near the C-terminus of hybO on the membrane facing side of [HybOC]₂ (right) suggest possible locations for interactions with other subunits in the physiologically relevant hybOCAB complex.